Ion Temperature from Tangential Charge Exchange Neutral Analysis on the Tokamak Fusion Test Reactor

PPPL--2476

DE88 003461

C.L. Fiore

Plasma Fusion Center, M.I.T.

Cambridge, MA 02139, USA

S.S. Medley, G.W. Hammett, R. Kaita, A.L. Roquemore, S.D. Scott

Plasma Physics Laboratory, Princeton University

Princeton, NJ 08544, USA

Abstract

Fokker-Planck simulations of the Tokamak Fusion Test Reactor (TFTR) energetic ion mode discharges were performed to evaluate the utility of deriving the central ion temperature, T_i, from deuterium neutral beam charge exchange spectra above the neutral beam injection energy. The T_i values obtained from fitting the calculated spectra obtained from sightlines nearly tangent to the neutral beam injection radius reproduce the central ion temperature within $\pm 10\%$ over the full range of TFTR energetic ion mode parameters. The code simulations demonstrate that the ion temperature obtained from the high energy tangential deuterium charge exchange spectrum is insensitive to variations in the plasma density, Z_{eff}, plasma current, loop voltage, and injected neutral beam power and energy. Use of this method to reduce charge exchange data from TFTR energetic ion mode plasmas is demonstrated.

1. Introduction

Recent experiments using high power ($\leq$ 18 MW) deuterium neutral beam injection into low density Tokamak Fusion Test Reactor (TFTR) deuterium plasmas have produced an energetic ion mode of operation [1]. The central ion temperatures for these plasmas measured by Doppler broadening of the FeXXV K_α line are in excess of 22 keV [2]. Charge exchange ion temperature measurements[3] of the bulk plasma are difficult to obtain from residual hydrogen in the deuterium plasma because of the low hydrogen concentration, which is typically $H/(H+D) \sim 1.5\%$. The deuterium charge exchange neutral energy spectra are dominated by the deuterium neutral beam slowing-down spectra rather than a thermal Maxwellian energy distribution, so that a method of obtaining the central ion temperature from the fast deuterium neutral spectra is desired.

In this work the feasibility of obtaining the central ion temperature of the TFTR plasma from the deuterium charge exchange neutral energy spectrum fitted above the neutral beam injection energy is explored. The solution to the Fokker-Planck equation in cylindrical geometry for beam ions near but above the neutral beam injection energy is of the form[4] $f(E) \sim \exp(-E/T_{eff})$, where

$$T_{eff} = \frac{T_i + (\frac{E}{E_c})^{1.5} T_e}{1 + (\frac{E}{E_c})^{1.5} \pm \tau_s 9.58 \times 10^{11} \frac{Z_b}{A_b} \frac{|\vec{E}^*|}{v_b} (\frac{E}{E_c})^{1.5}}. \quad (1)$$

In this equation T_i and T_e are the ion and electron temperatures, Z_b and A_b are the charge and mass of the neutral beam ions, and E_c is the critical energy above which the effects of the electron drag on the beam ions are more important than the ion energy diffusion. E_c is defined as

$$E_c = A_b (\frac{[Z]}{A_i})^{2/3} 14.8 T_e \quad (2)$$

where

$$\frac{[Z]}{A_i} = \sum \frac{n_i}{n_e} \frac{Z_i^2}{A_i} \frac{ln\Lambda_i}{ln\Lambda_e}. \quad (3)$$

The remaining term in the denominator accounts for the effects of the toroidal electric field, where τ_s is the slowing-down time of the fast ions, v_b is the beam ion velocity, and $|\vec{E}^*| = |\vec{E}|(1 - Z_b/Z_{eff})$ where $|\vec{E}|$ is the magnitude of the electric field in Volts/cm. The term containing the electric field is small ($O \sim 10^{-2}$ compared to unity) and will be

neglected in the calculation of T_i from T_{eff}. Thus the slope of the ion energy distribution function above the neutral beam injection energy is determined by a balance between the energy diffusion of the ions and the electron drag, resulting in an effective temperature which is a weighted average of the ion and electron temperatures.

In principle, the electron temperature measured from other diagnostics [5,6] can be used in conjunction with the measured logarithmic slope of the deuterium charge exchange flux plotted as a function of energy above the neutral beam injection energy to obtain the ion temperature of the plasma. Figure 1 shows a Fokker-Planck calculation of a chord-integrated deuterium charge exchange spectrum obtained from a tangential analyzer sightline at the neutral beam injection radius for a typical TFTR energetic ion mode discharge. The highest energy component of the injected beam was 100 keV and the energy range from which T_{eff} will be fit is 120-160 keV.

The ion temperature determined in this manner will represent the central ion temperature if the neutral beam deposition is near the plasma center (thus assuring that the neutral beam slowing down spectra results from collisions with plasma ions from the center of the plasma) and if the measured charge exchange neutral flux arises from the plasma center. The limits of plasma operating conditions for which these constraints are met so that the T_i calculated from T_{eff} corresponds to the central value to within $\pm 10\%$ error must be evaluated.

The analysis above applies in the limit of $v_\parallel/v = \pm 1$ and for E near the neutral beam injection energy, E_{beam}. In TFTR the neutral beam power is injected from 12 neutral beam sources, each aimed at a slightly different tangency radius. Also, the charge exchange flux reaching the analyzer from a given sightline is integrated over a number of $v_\parallel/v$ values relative to the tangency radii of the neutral beam injectors. Errors in the ion temperature derived from the slope of the deuterium charge exchange spectrum above the neutral beam injection energy could arise from deviation of the viewing sightline from the neutral beam injection tangency radius. An optimum charge exchange sightline selected to minimize this source of error must be determined.

Even though the derivation of Eq. (1) was done in the limit of $v_\parallel/v = \pm 1$, the pitch angle scattering operator should be insensitive to energy at the high ion energies considered

in this study. Therefore, deviation of the charge exchange analyzer sightline from the mean neutral beam injection tangency should not have a strong effect on the measured value of T_{eff}. However, the intensity of the charge exchange flux arising from a particular sightline will be a strong function of the proximity to the injection radius.

Variation in the neutral beam injection energy, differences in co- and counter-moving energetic ion orbits, noncentral origin of charge exchange signal, or excessive attenuation of the charge exchange signal could result in errors in the determination of the central ion temperature from T_{eff}. In this work these sources of error will be examined using the Fokker-Planck code FPPRF [7] to calculate the expected charge exchange spectra for TFTR operating parameters characteristic of the energetic ion mode in order to ascertain the range of discharge conditions suitable for ion temperature measurement from the slowing-down spectra of the neutral beams.

2. Plasma Parameters used in the Code Simulation

A typical TFTR energetic ion mode shot was selected to provide baseline code input parameters for the Fokker-Planck calculations of the charge exchange neutral energy spectra. These plasmas have a major radius of 2.45 m and minor radius of 0.8 m. The chosen parameters where $n_e(r) = 7.5 \times 10^{19} \times (1 - r^2/a^2)^4 \mathrm{m}^{-3}$, $T_e(r) = 6 \times (1 - r^2/a^2)$ keV, $T_i = 20 \times (1 - r^2/a^2)$ keV, $Z_{eff} = 3.5$, $A_{impurity} = 20$, $Z_{impurity} = 10$, $I_{plasma} = 0.85$ MA, $V_{loop} = 0.1$ V, and $B_{toroidal} = 5$ T with 10.5 MW neutral beam power at an energy of 100 keV. The neutral density profile was calculated with the FRANTIC code[8] and is a cylindrically symmetric function of minor radius with a central value of $n_0 = 1.5 \times 10^{12} \mathrm{m}^{-3}$ and an edge value of $n_0 = 5 \times 10^{14} \mathrm{m}^{-3}$. Variations from these baseline parameters were made to determine the sensitivity of the ion temperature derivation to changes in plasma discharge parameters. Table I lists the plasma parameters which were explored in this study. For most of the code simulations, the neutral beam power was distributed equally among 12 injection tangency radii varying from 1.73 m to 2.25 m, and was assumed to be fully balanced between the co and counter directions with 24 MW unless otherwise noted. The effects of co versus counter neutral beam injection as well as variations in the energy and power of the neutral beams were also investigated.

The viewing geometry for the TFTR horizontal charge exchange analysis is shown in

Fig. 2. The positive viewing radius is defined such that neutrals with $v_{\|}/v > 0$ (representative of co-moving ions, ions travelling in the direction of the plasma current) are detected while the negative sightline sees counter-moving particles.

3. Calculation of T_i from T_{eff}

T_{eff} is determined from measurement of the charge exchange flux at energies above the neutral beam injection energy and is given by

$$\frac{1}{T_{eff}} = \frac{d}{dE}\left[ln(\frac{1}{\sqrt{E}}\frac{dn}{dE})\right]. \tag{4}$$

The value of Ti calculated from the slope of the distribution function above the neutral beam injection is dependent upon the electron temperature and the average charge to mass ratio of the plasma. From Eq. (1), neglecting toroidal electric field effects,

$$T_i \approx T_{eff} + (T_{eff} - T_e)(E/E_c)^{3/2}. \tag{5}$$

The second term in Eq. (5) varies as a function of plasma radius due to the dependence on the electron temperature. Figure 3 shows the dependence of $(E/E_c)^{3/2}$ with radius for E=140 keV (the midpoint of the energy range from which T_{eff} will be calculated) for T_{e0} values from 4 to 10 keV with a radial profile represented by $T_{e0}(1 - r^2/a^2)^2$. The value of $(E/E_c)^{3/2}$ used in the code simulations corresponds to T_{e0} = 6 keV and is ~1.5-2.0 at $r/a < 0.4$ and increases rapidly at larger radii. The calculation of T_i from T_{eff} is thus insensitive to the point from which T_e is taken near the center of the plasma, but changes too rapidly with position at larger radii to be used to extract T_i without a full Fokker-Planck code analysis. This point is further illustrated in Fig. 4, which shows the ion temperature, electron temperature, and T_{eff} radial profiles expected from a typical TFTR high ion temperature shot. T_{eff} lies halfway between T_i and T_e near the plasma center but rapidly approaches T_e at $r/a > 0.5$. This imposes the restriction that the data must arise from the plasma center in order to utilize a simple interpretation of the high energy slope of the charge exchange neutral spectra.

The difference between T_i and T_{eff} decreases with increasing electron temperature, and $T_i = T_{eff}$ when $T_i = T_e$. Fig. 5 shows T_{eff}/T_i as a function of T_e/T_i for several values of T_e. The TFTR high ion temperature operating regime lies approximately between

$T_e = 5$ keV and $T_e = 10$ keV, and between $T_i = 5$ keV and $T_i = 30$ keV. Note that T_{eff}/T_i approaches unity as T_e becomes large.

4. Sensitivity to Geometrical Effects

Derivation of the central ion temperature from the slope of the charge exchange neutral energy spectrum above the neutral beam injection energy can be affected by several geometrical factors. First, the formula used to determine T_i from T_{eff} was obtained in the limit of $v_{\parallel}/v = \pm 1$, so that the charge exchange analyzer sightline chosen for this analysis should be tangent at the neutral beam injection radius. In TFTR the 12 neutral beams are injected at different tangency radii, ranging from 1.75 m to 2.25 m, and are injected from both the co and counter directions. Secondly, as noted above, it is important that the data obtained from the charge exchange neutral analyzer arise from the center of the plasma in order to simplify the interpretation of the data. Finite ion orbit effects and the radial distribution of the background neutral density could cause the charge exchange signal to originate from the outer part of the plasma.

4.1 Choice of Sightline

Selection of an optimal viewing tangency for the horizontal charge exchange analyzer is dependent on several criteria. The chosen view should yield data which reproduce the central ion temperature for the widest possible variation of TFTR plasma parameters. This criterion is met by selection of a viewing tangency as near as possible to the average neutral beam injection angle, which is 1.99 m for the balanced injection cases considered here. Also, the available neutral flux should be maximized in the range where T_{eff} is measured, in order to give the highest possible signal-to-noise ratio. This can also be achieved by selecting a view which is tangent to the neutral beam injection. Finally the neutral particle flux obtained from the chosen sightline should originate from the central plasma region ($r/a < 0.4$).

The Fokker-Planck code was used to calculate the charge exchange spectra over a range of analyzer tangency radii from +2.5 m to -2.5 m for the typical TFTR shot described in Sec. 2. At each tangency radius indicated by the plotted points in Fig. 6, a spectrum similar to that shown in Fig. 1 was generated by the Fokker-Planck code, and T_{eff} was derived from the slope of the spectrum above the injection energy. T_{eff} obtained from

the code calculations is shown as a function of sightline in Fig. 6. The ion temperature, T_i, was calculated from Eq. (5) using T_{eff} with T_e and E_c taken from $r/a = 0.1$ and is included in that figure. The lower error bar on the ion temperature used T_e and E_c from $r/a = 0$, and the upper from $r/a = 0.2$. The calculated ion temperature is within $\pm$ 10% of the input ion temperature (indicated by the dashed lines in Fig. 6) for most choices of viewing radius, with the exception of the sightlines near +2.0 m. As will be discussed in Sec. 4.2, the use of T_e and E_c from a slightly larger value of $r/a \sim 0.34$ is required to yield a calculated T_i value within 10% of the input value for the +2.0 m sightline.

The expected flux of neutrals at the charge exchange analyzer is shown in Fig. 7 as a function of viewing radius. This calculation was done for the same plasma parameters as the previous figure, but with 12 MW neutral beam power. Three cases are presented: the calculated flux for co-injected neutral beams only; counter-injected neutral beams only; and for fully balanced injection. The high energy flux at the analyzer is maximized near the average neutral beam injection radius for the balanced case at a viewing radius of $\pm$2.0 m. The neutral particle flux from positive (co-viewing) radii is dominated by the co-injected neutral beam, and the flux from the negative views is predominately from the counter-injected beam.

4.2 Source of Neutral Particle Flux

It is important in this analysis that the high energy neutral flux measured by the charge exchange analyzer originates in the central region of the plasma in order to provide a measure of the central ion temperature and to insure that the uncertainty arising from the choice of T_e used in the calculation of T_i from T_{eff} is small. The Fokker-Planck code was used to calculate the neutral particle flux originating from nested shells in the plasma minor cross section along with the attenuation of the flux exiting the plasma in order to determine the spatial origin of the expected charge exchange signal. This shell-by-shell flux calculation, which was made using the baseline TFTR discharge parameters, is shown in Fig. 8 for the $\pm$2.0 m viewing sightline at an energy of 128 keV and 160 keV. The flux is peaked just outside of center for the -2.0 m view and arises from a mean radius of $< r/a >= 0.29$ at 128 keV, and $< r/a >= 0.2$ at 160 keV. The origin of the flux seen from the +2.0 m view is somewhat outside the plasma center, with a mean value from

$< r/a >= 0.43$ at 128 keV and $< r/a >= 0.26$ at 160 keV.

The asymmetry in the positive versus negative charge exchange sightlines is related to differences between the co and counter beam ion trajectories, and is reduced for higher plasma currents. The percentage difference between T_{eff} obtained from the -2.0 m sightline and that obtained from the +2.0 m view as a function of the plasma current is shown in Fig. 9. T_{eff} determined from the calculated ion energy spectrum from the -2.0 m sightline does not change with increasing plasma current, while that obtained from the +2.0 m sightline increases with increasing current. This results in a 12% difference between the T_{eff} values obtained from the two sightlines at 0.85 MA which decreases to 1.5% at 2 MA.

The mean radii for the origin of the charge exchange flux at 128 keV and at 160 keV for the ± 2.0 m sightlines are plotted as a function of plasma current in Fig. 10. This plot suggests that T_e used to calculate T_i from T_{eff} should be taken from $0.1 < r/a \leq 0.29$ for the -2.0 m sightline. The value of r/a from which the T_e should be determined for analyzing the charge exchange flux obtained from the +2.0 m sightline should be $r/a = 0.4$ for the lowest value of plasma current and from decreasing r/a values to $r/a = 0.25$ with increasing plasma current.

4.3 Neutral Density Profile Effects

The neutral density profile used for the charge exchange source in these calculations is poloidally symmetric with $n_0 = 5 \times 10^{14}\mathrm{m}^{-3}$ at the edge and $n_0 = 1.5 \times 10^{12}\mathrm{m}^{-3}$ at the center. The arrangement of limiters in TFTR could alter the assumption of poloidal symmetry in this calculation. A toroidal limiter is located at the inboard wall of the vacuum vessel, and a movable limiter is situated at one toroidal location at the outer plasma edge[9]. When the plasma is in contact with only the toroidal limiter, the neutral density should peak at the inside plasma edge and should be only a weak function of radius in the outer part of the plasma[10]. This will not affect the localization of the charge exchange neutral signal for the -2.0 m viewpoint which already originates primarily from the center of the plasma. The +2.0 m viewpoint will become more centrally localized if the neutral density profile is peaked toward the inboard periphery of the plasma, since the contribution to the signal from the outer part of plasma is reduced relative to that from the plasma center. This is evident from comparing the symmetric neutral density

results of Fig. 6 with Fig. 11, which shows T_{eff} and T_i as a function of viewing sightline calculated with a rising neutral density profile toward the inner periphery of the plasma and a flat profile outboard of the plasma core, $R > R_0$.

As the plasma density is increased, cold neutrals from the plasma edge penetrate less into the plasma, giving rise to a steep gradient in the neutral species profile. In thermal charge exchange experiments this edge-enhanced neutral density profile gives extra weight to charge exchange neutrals arising from the lower temperature plasma edge[11]. Use of the neutral beam slowing-down spectra diminishes this effect because the source of the high energy ions is localized to the region where the neutral beam ions are deposited. The neutral beam deposition does occur at slightly larger values of r/a at the highest densities considered here. The mean value of r/a shifts outward by 18% for the -2.0 m sightline and 30% for the +2.0 m sightline for the highest density case ($\bar{n}_e = 1.5 \times 10^{20} \mathrm{m}^{-3}$.)

The neutral particle flux from both the +2.0 m and -2.0 m sightlines has been shown to originate predominately in the central region of the plasma. The slight asymmetry found in the origin of the charge exchange flux between the +2.0 m and -2.0 m sightlines is most severe for the assumptions made in the baseline calculation. The asymmetry is reduced as the plasma current is increased, and if the contribution from neutral particles at the outer plasma edge is reduced.

5. Sensitivity to Plasma Parameters

This method of calculating the central ion temperature from the measured effective temperature can only be used on a routine basis if it is insensitive to variations in the TFTR plasma discharge conditions other than the ion and electron temperatures. The charge exchange spectra were calculated for viewing tangency radii of ± 2.0 m using the baseline TFTR discharge parameters and changing only the value of the central ion temperature, which was varied from 4 keV to 30 keV. The calculated value of T_i determined from the slope of the spectrum above the neutral beam injection energy is shown in Fig. 12a, using a T_e value taken from $r/a = 0.1$ for the -2.0 m sightline and from $r/a = 0.34$ for the +2.0 m sightline. The T_i determined from T_{eff} is within 10% of the input value for the entire range of input ion temperature.

This series of code simulations was repeated for variations in a single plasma param-

eter, the other plasma parameters remaining fixed at the baseline values, in order to test for errors induced by changes in the plasma operating conditions.

5.1 Electron Density and Z_{eff}

Changes in the electron density alter the neutral beam deposition in the plasma and the attenuation of the neutral particle flux as it exits the plasma, possibly causing a shift in the point of origin of the charge exchange flux. The simulations were done with central electron densities varying from $5 \times 10^{19}\mathrm{m}^{-3}$ up to $1.5 \times 10^{20}\mathrm{m}^{-3}$ with a peaked density profile typical of TFTR energetic ion mode plasmas, $(1-r^2/a^2)^4$. The values of calculated ion temperature were slightly lower for the highest density cases than for the baseline case, but remained within $\pm 10\%$ of the input value using T_e taken from $r/a = 0.1$ for the -2.0 m sightline, while the values obtained for the +2.0 m sightline obtained using T_e taken from $r/a = 0.34$ were about 20% lower than the input T_i (Fig. 12b). The calculation was also done for a broader density profile, $7.5 \times 10^{19}(1-r^2/a^2)\mathrm{m}^{-3}$, with little change observed in the calculated T_i (Fig. 12c).

The value of Z_{eff} affects the rate of pitch angle scattering of the high energy ions as well as the hydrogenic ion fraction of the plasma. A series of calculations were done with the baseline plasma parameters in which Z_{eff} was varied from 2.5 to 4.5. The calculated T_i values generally fall within 10% of the input ion temperature using T_e from the values of r/a noted previously for the full range of ion temperatures sampled (Fig. 12d) and over all Z_{eff} values in this range.

5.2 Plasma Current

The plasma current used for the TFTR baseline case, 0.85 MA, is near the minimum used in neutral-beam-heating experiments. As noted in Sec. 5, increasing the plasma current affects the origin of the charge exchange flux for the positive viewing radii, causing it to be more centrally weighted for higher currents. The plasma current was varied from the baseline case up to 2 MA. The ion temperature calculated as a function of viewing sightline is shown in Fig. 13 for 1.9 MA plasma current. This demonstrates that the temperature derived from positive and negative sightlines is much more symmetric than in the baseline case (Fig. 6). The value of T_i calculated from the negative views was unaffected by changing plasma current and remained within 10% of the input value for the

full range of input ion temperatures using the previous T_e value, arising from $r/a = 0.1$. The values of T_i calculated from the positive viewpoint were within 10% of the input value (Fig. 14) if T_e was taker from the smaller value of $r/a = 0.2$ than had been used at lower plasma current.

5.3 Electric Field Effects

The derivation of the central ion temperature from the slope of the charge exchange spectra above the maximum neutral beam injection energy is done assuming that the parallel electric field can be neglected. For typical TFTR operating parameters this leads to a possible error in T_i of 1%. However, the effects of the electric field are fully included in the Fokker-Planck code calculations of the neutral energy spectra. The loop voltage for the energetic ion mode used as the baseline case is 0.11 V. Increasing the loop voltage by a factor of 10 to 1.1 V decreases the ion temperature determined from the -2.0 m sightline by 8.5% and increases the ion temperature from the +2.0 m sightline by 10%. The derived ion temperature for the two cases is shown as a function of viewing sightline in Fig. 15. Neglect of the electric field even for large changes in the loop voltage of TFTR imposes less than 10% error in the ion temperature calculated from the high energy deuterium spectrum.

6. Sensitivity to Neutral Beam Parameters

The high energy deuterium neutral particle flux detected by the charge exchange analyzers derives almost entirely from neutral beam ions. It is expected that changes in the neutral beam parameters will affect the relative charge exchange flux.

The charge exchange spectra from TFTR baseline discharges were calculated with the Fokker-Planck code for neutral beam injection powers ranging from 12 MW up to 27 MW. The T_i values calculated from T_{eff} fell within 10% of the input ion temperatures over the full range of neutral beam powers (Fig. 16b) using T_e values taken from $r/a = 0.1$ for the -2.0 m data and from $r/a = 0.34$ for the +2.0 m sightline.

Small variations in the neutral beam injection energy could affect the value of the slope of the neutral beam slowing-down spectrum in the region where the T_{eff} fit is determined. Charge exchange spectra were calculated for typical variations of $\pm 10\%$ in the neutral beam injection energy for several different cases. In one case, four of the beams were

injected with 95 keV, four with 100 keV, and four with 105 keV. Another variation was tested using all of the counter-injected beams at 90 keV and all of the co-injected beams at 100 keV. A third calculation was done with eight of the beams at 90 keV and four at 100 keV. The most extreme deviation of the calculated T_i from the input value was found (Fig. 16c) when four of the beams were injected with 90 keV, four with 100 keV, and four with 110 keV. Even in this case the calculated T_i value fell within 10% of the input value.

The high energy neutral particle flux accepted by a charge exchange analyzer with a positive sightline is primarily from co-injected neutral beams and that detected from a negative sightline is primarily from the counter-injected neutral beams. The ion temperature derived from the high energy charge exchange spectrum for all co (from the +2.0 m sightline) or all counter neutral beam injection (for the -2.0 m sightline) as a function of input ion temperature is shown in Fig. 16d. The calculated ion temperature is within 10% of the input value for the full range of ion temperatures. The calculated ion temperature is also within 10% of the input value for the cases of a co-viewing sightline with all counter-injection and for a counter-viewing sightline of all co-injection. However, the absolute value of the charge exchange flux is greatly reduced in those cases.

The ion temperature calculated from T_{eff} is insensitive to the total neutral beam injection power and to $\pm 10\%$ variations in the mean neutral beam energy. It is also not sensitive to whether the neutral beams are injected in the co or counter directions.

The solution to the Fokker-Planck equation which yields Eq. (1) was solved as a linear problem by assuming that the slowing-down beam ions suffer energy diffusion through collisions only with a Maxwellian thermal population. At low plasma current ($I_p \leq 1.1$ MA), high beam power ($P_b = 10 - 20$ MW) operation in TFTR, the calculated ratio of beam ion density to thermal deuteron density at the plasma center can reach 1:3 during balanced injection, and even 1:1 during unidirectional co-injection. Under these conditions a nonlinear solution to the Fokker-Planck equation may be required, which incorporates energy diffusion of beam ions through collisions with other beam ions. The nonlinear effects are beyond the scope of this analysis, and will be addressed in a later work.

7. Application to TFTR

In the course of the TFTR operating period from January to July of 1987, charge

exchange measurements were made during deuterium neutral beam heating of deuterium plasmas to explore the application of this technique for obtaining central ion temperature measurements from fast ion spectra as described in this paper. A mass- and energy-resolving $E||B$ charge exchange analyzer [12,13] was used which was remotely scannable, enabling the sightline to cover a range of tangency radii from R_{tan} = 0.36–2.14 m in the horizontal midplane. This analyzer is designated as EH 4 in Fig. 17, which shows the arrangement of the horizontal (EH) and vertical (EV) charge exchange analyzer arrays on TFTR relative to the neutral beam injectors. Of the three horizontal analyzers, only EH 4 was equipped with a shield to suppress neutron- and gamma-induced noise signals in the microchannel plate detector [14]. Consisting of lead(~10 cm thick) nested inside borated polyethylene (~30 cm thick), the shield provided a 140 times reduction in the noise level relative to the unshielded analyzers.

Charge exchange results will be presented for two neutral-beam-heating cases which are distinguished primarily by the presence of high ($|\vec{v}_\phi| = 6.8 \times 10^5$ m/s, Case I) and low ($|\vec{v}_\phi| = 1.5 \times 10^5$ m/s, Case II) plasma toroidal rotation velocity. The tangency radius of the analyzer sightline was R_{tan} = +2.0 m for both cases. Some parameters characterizing the discharges are listed in Table II. The charge exchange data will be compared with measurements from the horizontal X-ray crystal diagnostic [15] which used the Doppler broadening of the NiXXVII K_α impurity line emission to obtain central plasma ion temperatures.

7.1 Case I: High Toroidal Rotation

Since the existence of a high plasma toroidal rotation velocity presents the most severe condition for application of this technique, this case will be discussed in detail. Co-injection only was used in this discharge with neutral beam sources 3A, 3B, 3C, 4B, and 4C (see Fig. 17), delivering a total injected deuterium neutral beam power of P_b = 10 MW. The full energy ranged from 90 keV to 105 keV with a mean value of $< E_{inj} >= 95$ keV. The beams were injected from 4.0-6.0 seconds into a toroidally limited, low density ($\bar{n}_e = 0.6 \times 10^{19}\mathrm{m}^{-3}$) deuterium plasma. Following beam turn-on, the central toroidal rotation velocity rose rapidly to $|\vec{v}_\phi| \sim 1 \times 10^6 m/s$, but fell abruptly to $|\vec{v}_\phi| = 6.8 \times 10^5 m/s$ at t=4.4 s and remained constant at this value for the duration of the beam pulse.

The measured deuterium spectra in the energy range of 50-200 keV is shown in Fig. 18 as a function of time during the 2 s neutral-beam-heating pulse. The charge exchange data were acquired with a time resolution of 30 ms. A correction for the residual neutron- and gamma-induced noise signal was also applied during the analysis. Noise correction is facilitated by using "masked" detectors which respond only to the neutron and gamma radiation to monitor the noise level as a function of time during the discharge. Using the relative neutron/gamma sensitivity of the individual charge exchange signal channels to the masked detectors determined by prior calibration, a time-dependent correction for noise on the raw charge exchange signal is obtained.

A time-slice from this spectrum at t= 5.5 s shown in Fig. 19 illustrates two important features of the charge exchange spectra which are generally observed in the application of this technique. First, at energies modestly above the indicated mean injection energy the semi-logarithmic spectrum exhibits a linear behavior which extends to a maximum energy imposed by signal-to-noise considerations. In this example, a linear least-squares fit to the data (open circles) in the energy range of 124-187 keV yields a measured value of $T_{eff} \approx 16.2$ keV. Secondly, the amplitude of the charge exchange spectrum extends almost four e-foldings above the neutron noise level. Such strong signal levels are a significant experimental advantage of this technique. In fact with increasing injected beam power the signal and the neutron noise levels both increase, which tends to preserve the favorable signal-to-noise ratio.

The results of the analysis of the charge exchange data obtained by application of the procedures developed from the Fokker-Planck simulations and the toroidal rotation analysis (Appendix A) are shown in Fig. 20. The lower three curves provide reference waveforms for the total injected beam power, P_b (MW), the line-integral electron density measured in the horizontal midplane with the 1-mm interferometer, $n_e l(\times 10^{19} \mathrm{m}^{-2})$, and the time evolution of the central electron temperature, $T_e(keV)$, obtained by renormalizing the Michelson interferometer waveform to the Thomson scattering data at t=5.5 s. A parabolic-squared $T_e(r)$ profile was assumed, and the E_c, T_e values required in Eq. (5) were evaluated at $r/a = 0.34$ as prescribed by the Fokker Planck simulation results for the +2.0 m analyzer sightline. The upper dashed curve shows the results of the analysis

without correction for toroidal rotation effects. Application of the toroidal correction following the procedure given in Appendix A yields central ion temperatures from the charge exchange method shown by the solid data points. The toroidal rotation velocity in this example, $|\vec{v}_\phi| = 6.8 \times 10^5$ m/s, is close to the maximum observed during neutral-beam-heating experiments on TFTR to date [16]. Thus, for unbalanced neutral-beam-heating experiments on TFTR, toroidal rotation corrections to the central ion temperature obtained by this charge exchange method are substantial, with corrections in the range of 50% at the highest rotation speeds. Nevertheless, it is evident that reasonable agreement is found between the charge exchange results, which include the correction for toroidal rotation, and the central ion temperatures obtained from the horizontal X-ray crystal Doppler-broadening diagnostic (open data points). Preliminary analysis of an extended database consisting of approximately 70 shots covering a wide range of beam power ($P_b \sim$ 2-18 MW) and toroidal rotation speed ($v_\phi \sim 1 - 8 \times 10^5$ m/s), which is in progress, continues to support this agreement.

7.2 Case II: Low Toroidal Rotation

The combined effects of balanced neutral beam injection and a higher electron density, both before and during the neutral beam pulse, lead to a relatively low toroidal rotation velocity for the discharge in this case with $|\vec{v}_\phi| \leq 1.5 \times 10^5 m/s$ throughout the 1.5 s heating pulse. The charge exchange data were analyzed in the same manner as discussed in Case I, but without inclusion of toroidal rotation corrections. As shown in Fig. 21, the derived central ion temperature from charge exchange (solid data points) is in agreement with the X-ray crystal Doppler-broadening measurement (open data points). Application of the procedure given in Appendix A yields a toroidal rotation correction to the charge exchange ion temperature of 7% for this case. The bars on the charge exchange data points in this plot show the variation in the derived ion temperature which results from imposing a ± 0.1 change in the value of $r/a = 0.34$ used to determine the magnitude of T_e and E_e in Eq. (5).

The above examples illustrate that the charge exchange method advanced in this paper yields central ion temperature measurements which appear to be reliable, based on the agreement to within $\pm 10\%$ with data from the X-ray crystal Doppler-broadening

diagnostic. Although substantial corrections to the charge exchange data are required for discharges having high toroidal rotation velocity, a simple but adequate procedure has been developed to correct for this effect.

8. Conclusions

This study has demonstrated that the central ion temperature can be extracted from the deuterium charge exchange spectrum obtained during deuterium neutral beam injection in TFTR energetic ion mode discharges. It has been shown that data obtained from sightlines at the mean tangency radius of the neutral beam injectors originate near the plasma center for typical TFTR operating parameters. The central ion temperature is well reproduced despite wide variations in input plasma parameters. The calculated T_i values fall within 10% of the input values for central plasma density variations from $5 \times 10^{18}\mathrm{m}^{-3}$ to $1.5 \times 10^{20}\mathrm{m}^{-3}$, density profiles of $(1 - r^2/a^2)^{\alpha}$ where α varies from 1 to 4, $2.5 < Z_{eff} < 4.5$, and plasma currents ranging from 0.85 MA to 2 MA. The calculated T_i values were insensitive to neutral beam power changes from 12 MW to 27 MW or to $\pm 10\%$ changes of the neutral beam injection energy about a mean value. Application of this technique to high energy charge exchange data from TFTR energetic ion mode plasmas yields ion temperature values which are in agreement with those obtained using other diagnostic methods.

Appendix A: Toroidal Rotation Effects

In TFTR the introduction of unbalanced neutral beam injection can induce large plasma toroidal rotation velocities. Rotation speeds of up to 8×10^5 m/s have been observed. The velocity of an ion in the rotating plasma is different from the velocity of the same ion detected by the charge exchange analyzer, both in magnitude and direction. This affects assumptions made about the relative importance of the electron collisional effects in the determination of the distribution function. In addition, the slope of the measured ion energy distribution function is modified from its plasma frame value by the rotation.

Toroidal rotation effects have not been included in the Fokker-Planck code used in this study. The purpose of this appendix is to estimate the importance of the toroidal rotation effects in interpreting charge exchange data, and to provide a method of correcting for them.

A.1 Basis for Rotation Correction

An energetic neutral hydrogen atom having a velocity $\vec{v}_i$ exiting a plasma which rotates toroidally with velocity $\vec{v}_\phi$ has a velocity $\vec{v}_{lab}$ with respect to the charge exchange analyzer given by

$$\vec{v}_{lab} = \vec{v}_i + \vec{v}_\phi. \tag{A1}$$

The measured energy of this neutral, $E_{lab} = \frac{1}{2} m_i |\vec{v}_{lab}|^2$ where m_i is the ion mass, is different from its energy E_i in the plasma frame,

$$E_i = E_{lab} - 2cos(\theta)\sqrt{E_{lab}E_\phi} + E_\phi. \tag{A2}$$

Here E_ϕ is defined $\frac{1}{2} m_i |\vec{v}_\phi|^2$ and θ is the angle between the charge exchange analyzer sight-line and the direction of the plasma rotation. This energy in the plasma frame determines the effective temperature in the plasma frame,

$$T'_{eff} = \frac{T_i + (\frac{E_i}{E_c})^{1.5} T_e}{1 + (\frac{E_i}{E_c})^{1.5}}. \tag{A3}$$

The distribution function in the laboratory frame is related to the distribution function in the plasma frame by

$$f(E_{lab}) = f(E_i)\frac{dE_i}{dE_{lab}} = \left(1 - cos(\theta)\sqrt{\frac{E_\phi}{E_{lab}}}\right) e^{-E_i/T'_{eff}}. \; eqno(A4)$$

If the distribution function in the lab frame is approximated by $\tilde{f}(E_{lab}) = Ae^{-E_{lab}/T_{lab}}$ where A is an energy dependent constant, then in the manner of Scott[17] minimization of the error integral

$$\epsilon(T_{lab}) = \int_{E_1}^{E_2} dE \left(ln\left(\frac{f(E, T'_{eff})}{\sqrt{E}}\right) - ln\left(\frac{\tilde{f}(E, T_{lab})}{\sqrt{E}}\right)\right)^2 \tag{A5}$$

with respect to T_{lab} will yield an expression for T_{lab} in terms of T'_{eff}. The limits of integration in this case are the energies from which the slope of the measured distribution function will be fit to obtain T_{lab}. The result is

$$T_{lab} = \frac{T'_{eff}}{1 - cos(\theta)F(a,b)\sqrt{\frac{E_\phi}{T'_{eff}}}} \tag{A6}$$

where a and b are determined by the integration limits, $E_1 = aT'_{eff}$ and $E_2 = bT'_{eff}$, and

$$F(a,b) = \frac{12(b^{2.5} - a^{2.5}) - 10(b^{1.5} - a^{1.5})(a+b)}{5(b^3 - a^3) - 3.75(b^2 - a^2)(a+b)}. \quad (A7)$$

Figure 22 shows $F(a,b)$ for ranges of a,b appropriate for neutral-beam-heated TFTR discharges.

Another effect stemming from the toroidal plasma rotation results from the fact that the angle of the velocity of the ions detected by the charge exchange analyzer is fixed, so that the angle between the ion velocity and the neutral beam velocity is different in the plasma and laboratory frames. The angle between the velocity of the escaping neutrals which are detected by the charge exchange analyzer and the direction of neutral beam injection is derived from $\vec{v}_b \cdot \vec{v}_i$ and is given by

$$cos(\theta_{ib}) = \frac{cos(\theta_{lb})\sqrt{E_{lab}} - cos(\theta_{b\phi})\sqrt{E_\phi}}{\sqrt{E_{lab} - 2cos(\theta)(E_\phi E_{lab})^{\frac{1}{2}} + E_\phi}}, \quad (A8)$$

where $\vec{v}_b$ is the neutral beam velocity, θ_{lb} is the angle between the neutral beam injection angle and the charge exchange analyzer sightline, and $cos(\theta_{b\phi}) = R_{tan}/R_0$ is the angle between the neutral beam injection and the plasma major radius.

A.2 Magnitude of the Rotation Correction

Consider the case described in Table I, used as the baseline data set for these calculations, where $T_{eff} = 9.7$ keV was found for the +2.0 m sightline. From the shell-by-shell study of the neutral particle source it was determined that E_c should be chosen from $T_e(r/a = 0.34)$, which in this case yields E_c =87.5 keV. If a spatially constant toroidal rotation is applied at a velocity $|\vec{v}_\phi| = 8 \times 10^5$ m/s, the effective energy of rotation will be E_ϕ =6.7 keV. The angle between the major radius and the charge exchange sightline is $cos(\theta) = 0.72$. Thus 140 keV ions in the laboratory frame will have a relative energy in the plasma frame of E_i =102.6 keV. This results in T'_{eff} =11.43 keV. For fitting this example, values of a and b are typically 18 and 15 respectively, which gives $F(a,b) = 0.28$. Application of Eq. (A6) yields T_{lab} = 13.41 keV. Use of this value to calculate T_i from Eq. (5) would result in T_i =29 keV, which is 45% higher than the 20 keV input ion temperature.

A rotation speed of $|\vec{v}_\phi| = 5 \times 10^5$ m/s, which is more typical of unbalanced neutral-beam-injected TFTR discharges, leads in a similar fashion to a 33% overestimate of the ion temperature.

Code simulation of the rotating case was done by injecting the co-going neutral beams at a reduced energy determined by $E = E_b - 2\sqrt{E_b E_\phi} + E_\phi$, which was 55 keV for $|\vec{v}_\phi| = 8 \times 10^5$ m/s and $E_b = 100$ keV. T_{eff} determined from the resulting distribution function using energy fit limits similarly reduced from those used in the nonrotating plasma was 9.9 keV rather than 11.43 keV as was estimated above. Several similar calculations using different values for $|\vec{v}_\phi|$ resulted in a maximum deviation in T'_{eff} from T_{eff} of 4%. This probably results from deposition of beam ions at larger major radii in the reduced energy simulations. This simulation represents one extreme in the analysis of the rotation problem because the plasma rotation in TFTR varies as a function of radius. As such, direct substitution of T'_{eff} for T_{eff} results in a lower limit for the toroidal rotation correction which must be applied to any charge exchange data obtained from a rotating plasma.

For an average neutral beam injection tangency radius of 2.0 m and a charge exchange analyzer sightline of 2.0 m, it can be seen from Eq. (A8) that the ions which are detected in the analyzer from a plasma rotating with $|\vec{v}_\phi| = 8 \times 10^5$ m/s deviate 10° from the neutral beam tangency radius, which is an effective sightline of 1.95 m. This small deviation does not significantly affect the determination of T_i from T_{eff} for this sightline.

Acknowledgements

The authors gratefully acknowledge M. Bitter and H. Hsuan for providing the Doppler broadening X-ray crystal ion temperature data presented in this report. We would also like to thank K. M. Young, L. C. Johnson, and the entire TFTR group for their support of this work.

This work was sponsored by the United States Department of Energy under Contract DE-AC02-78ET51013 and Contract DE-AC02-76CHO-3073.

References

[1]STRACHAN, J.D., BITTER, M., RAMSEY, A.T., ZARNSTORFF, M.C., ARUNASALAM, V., *et. al.*, Phys. Rev. Lett. **58** (1987) 1004.

[2]BITTER, M., HILL, K.W., COHEN, S., VON GOELER, S., HSUAN, H. *et. al.*, Rev. Sci. Instrum. **57** (1986) 2145.

[3]DAVIS, S.L., MUELLER, D., KEANE, C.J., Rev. Sci. Instrum. **54** (1983) 315.

[4]GOLDSTON, R.J., PhD Thesis, Princeton University (1977). A factor of $1/v_b$ in the electric field term inadvertently omitted in Eq. (29) has been included in our Eq. (1).

[5]JOHNSON, D., BRETZ, N., DIMOCK, D., GREK, B., LONG, D. , FALLADINO, R., TOLNAS, E., Rev. Sci. Instrum. **57** (1986) 1856.

[6]TAYLOR, G., EFTHIMION, P.C., MCCARTHY, M.P., FREDD, E., CUTLER, R.C., Rev. Sci. Instrum. **57** (1986) 1974.

[7]HAMMETT, G.W., PhD Thesis, Princeton University (1985); also GOLDSTON, R.J., PhD Thesis, Princeton University (1977); also CORDEY, J.G., Nucl. Fusion **16** (1976) 499.

[8]TAMOR, S.J., J. Comput. Phys. **40** (1981) 104.

[9]CECCHI, J., J. Nucl. Mater. **128-129** (1984) 1.

[10]HEIFETZ, D.B., LANGER, W.D., EHRHARDT, A.B., "Three Dimensional Calculations of the Transport of Neutral Hydrogen and Molecular Impurities in TFTR," (Proc. 12th European Conf. on Controlled Fusion and Plasma Physics, Budapest, 1985), Vol. 1, EPS (1985) 183.

[11]PARSONS, C.R., MEDLEY, S.S., Plasma Phys. **16** (1974) 267.

[12]ROQUEMORE, A.L., GAMMEL, G., HAMMETT, G.W., KAITA, R., MEDLEY, S.S., Rev. Sci. Instrum. **56** (1985) 1120.

[13]KAITA, R., HEIDBRINK, W.W., HAMMET, G.W., CHAN, A.A., ENGLAND, A.C., *et. al.*, Nucl. Fusion **26** (1986) 863.

[14]MEDLEY, S.S., PERSING, R., Rev. Sci. Instrum. **52** (1981) 1463.

[15]HILL, K.W., BITTER, M., TAVERNIER, M., DIESSO, M., VON GOELER, S., Rev. Sci. Instrum. **56** (1985) 1165.

[16]BITTER, M., ARUNASALAM, V., BELL, M.G., BOSCH, S., BRETZ, N.L.,

BUDNY, R., *et. al.*, "High Power Neutral Beam Heating Experiments on TFTR with Balanced and Unbalanced Momentum Input," (Proc. 14th European Conf. on Controlled Fusion and Plasma Physics, Madrid, 1987). To be published in Plasma Physics and Controlled Fusion.

[17]SCOTT, S.D. PhD Thesis, MIT 1983.

Table I. Plasma Parameters Used in the Simulations

TFTR High Ion Energy Mode Baseline Shot Based on #26608

$T_e(r) = T_{e0} \times (1 - r^2/a^2)^2$ keV, $T_{e0} = 6$keV

$T_i(r) = T_{i0} \times (1 - r^2/a^2)^2$ keV, $T_{i0} = 20$ keV

$n_e = n_{e0} \times (1 - r^2/a^2)^4$, $n_{e0} = 7.5 \times 10^{19}\mathrm{m}^{-3}$

$P_{beam} = 10.5$ MW (24 MW, balanced injection used in simulations)

$E_{beam} = 100$ keV

$Z_{eff} = 3.5$

$A_{imp} = 20$

$Z_{imp} = 10$

$n_0(r/a = 0) = 1.5 \times 10^{12}\mathrm{m}^{-3}$, $n_0(r/a = 1) = 5.5 \times 10^{14}\mathrm{m}^{-3}$, FRANTIC profile

$B_{toroidal} = 5.1$ T

$I_{plasma} = 0.85$ MA

$V_{loop} = 0.1$ V

Variation of Parameters Used in the Simulations

$T_e(r) = T_{e0} \times (1 - r^2/a^2)^2$ keV, $T_{e0} = 6$keV

$T_i(r) = T_{i0} \times (1 - r^2/a^2)^2$ keV, $4 < T_{i0} < 30$ keV

$n_e = n_{e0} \times (1 - r^2/a^2)^\alpha$, $5 \times 10^{19} < n_{e0} < 1.5 \times 10^{20}\mathrm{m}^{-3}$, $\alpha = 1$, $\alpha = 4$

12MW$< P_{beam} <$ 27 MW, balanced, all co, all counter

90keV$< E_{beam} <$ 110 keV, equal and mixed energies

$2.5 < Z_{eff} < 4.5$

$A_{imp} = 20$

$Z_{imp} = 10$

$n_0(r/a = 0) = 1.5 \times 10^{12}\mathrm{m}^{-3}$, $n_0(r/a = 1) = 5.5 \times 10^{14}\mathrm{m}^{-3}$, FRANTIC profile

$B_{toroidal} = 5.1$ T

0.85MA$< I_{plasma} <$ 2 MA

0.1V$< V_{loop} <$ 1.1 V

Table II. Plasma Parameters for the Experimental Results

Parameter	Case I (#31457)	CaseII (#30655)
I_p(MA)	0.9	1.1
B_t(T)	4.8	4.8
R(m)	2.45	2.45
a(m)	0.8	0.8
P_b(MW)	10.0	13.2
P_{co}(MW)	10.0	7.0
P_{ctr}(MW)	0.0	6.2
Cofrac*	1.0	0.06
$\|\vec{v}_\phi\|$(m/s)**	6.8×10^5	1.5×10^5
$\overline{n}_e$,target(m^{-3})	0.6×10^{19}	1.1×10^{19}
$\overline{n}_e$,beam(m^{-3})	1.6×10^{19}	2.8×10^{19}

*Cofrac=$(P_{co} - P_{ctr})/(P_{co} + P_{ctr})$ where P_{co}, P_{ctr} is the co– and counter–injected beam power respectively.

**Representative value during the neutral-beam-heating pulse.

Figure Captions

Figure 1. Fokker-Planck calculation of the deuterium charge exchange neutral spectrum from the -2.0 m viewing sightline during deuterium neutral beam injection for a baseline energetic ion mode discharge. $T_i = 20$ keV, $T_e = 6$ keV, $n_e = 7.5 \times 10^{19}(1 - r^2/a^2)^4 \mathrm{m}^{-3}$, $Z_{eff} = 3.5$, $I_{plasma} = 0.85$ MA, $P_{beam} = 24$ MW, $B_{toroidal} = 5.5$ T, $V_l = 0.11$ V.

Figure 2. Orientation of sightline tangency radii for charge exchange neutral code simulation on TFTR. Positive sightlines view co-going neutrals while negative sightlines see counter-moving neutrals. The plasma major radius is R_0 =2.45 m, and simulations were done for $-2.5 < R_{tan} < +2.5$ m.

Figure 3. The critical energy for determination of the relative contribution of the ion and electron temperatures to T_{eff} as a function of radius. $T_e = T_{e0}(1 - r^2/a^2)$, $T_{e0} = 4$, 5, 6, 8, and 10 keV, $E_0 = 140$ keV, $[Z]/A_i = 1/2$, $A_b = 2$.

Figure 4. $T_i(r)$, $T_e(r)$, $T_{eff}(r)$ for the baseline high ion energy mode discharge, showing the difference between T_{eff} and T_i as a function of plasma radius.

Figure 5. T_{eff}/T_i as a function T_e/T_i for T_e =1,5,9,13, and 17 keV, $T_e < T_i < 30$ keV. The hatched area shows the typical operating regime for neutral-beam-heated discharges in TFTR.

Figure 6. T_{eff} and T_i calculated from T_{eff} using T_e at $r/a = 0.1$ as a function of charge exchange analyzer viewing sightline. The lower error bar is from T_e for $r/a = 0$. and the upper error bar is with T_e from $r/a = 0.2$.

Figure 7. Natural logarithm of the calculated neutral particle efflux from the plasma as a function of viewing sightline at 128 keV for all co, all counter, and balanced neutral beam injection. $P_b = 12$ MW, $T_i = 12$ keV, and all other parameters are from the baseline TFTR energetic ion mode discharge.

Figure 8. Calculated neutral particle efflux from the plasma for the $\pm$ 2.0 m sightlines as a function of position of origin for 128 keV neutrals and 160 keV neutrals. All parameters are from the TFTR energetic ion mode baseline discharge. The mean origin of flux for the +2.0 m sightline is 2.72 m ($r/a = 0.43$) at 128 keV, and 2.58 m ($r/a = 0.26$) at 160 keV. The mean origin of flux for the -2.0 m sightline is 2.46 m ($r/a = 0.29$) at 128 keV, and 2.44 m ($r/a = 0.2$) at 160 keV.

Figure 9. Percentage asymmetry between T_{eff} calculated for ± 2.0 m sightlines as a function of plasma current. All other parameters are from the TFTR energetic ion mode baseline discharge.

Figure 10. Mean origin of the calculated neutral particle flux from the plasma for sightlines at ± 2.0 m at neutral energies of 128 keV and 160 keV as a function of plasma current.

Figure 11. T_{eff} and the ion temperature derived from T_{eff} as a function of viewing sightline calculated with an asymmetric neutral density source, having a maximum of $5 \times 10^{14}\mathrm{m}^{-3}$ at the inner plasma edge, decreasing to a minimum of $2 \times 10^{12}\mathrm{m}^{-3}$ at the plasma center, and extending to the outer plasma edge. All other parameters are from the TFTR energetic ion mode baseline discharge.

Figure 12. T_i calculated from T_{eff} as a function of the central ion temperature used in the Fokker-Planck calculation. T_i from the -2.0 m sightline are calculated with E_c and T_e from $r/a = 0.1$ and the +2.0 m sightline from $r/a = 0.34$. Plasma parameter scenarios correspond to a) the TFTR energetic ion mode baseline case, b) high electron density ($n_{e0} = 1.5 \times 10^{20}\mathrm{m}^{-3}$), c) broad electron density profile, $n_e = 7.5 \times 10^{19}(1 - r^2/a^2)\mathrm{m}^{-3}$, and d) $Z_{eff} = 4.5$. All unmentioned parameters for each case are from the TFTR energetic ion mode baseline discharge.

Figure 13. T_i calculated from T_{eff} as a function of viewing sightline for a plasma current of 1.9 MA. The values derived from the positive and negative sightlines are nearly symmetric. All other parameters are from the TFTR energetic ion mode baseline discharge.

Figure 14. T_i derived from T_{eff} as a function of the input value of T_i used in the Fokker-Planck calculation for a plasma current of 2 MA. All other parameters are from the TFTR high ion energy mode baseline discharge.

Figure 15. T_i calculated from T_{eff} as a function of viewing sightline for an artificially high loop voltage (1.1 V) case compared to the TFTR energetic ion mode baseline case with loop voltage 0.11 V. T_i obtained from the -2.0 m sightline is decreased 8.5% and T_i obtained from the +2.0 m sightline is increased 10% over the baseline discharge. All other parameters are from the TFTR energetic ion mode baseline discharge.

Figure 16. T_i derived from T_{eff} as a function of the input value of T_i used in the Fokker-Planck calculation for different neutral beam injection parameters. These are a) the TFTR

energetic ion mode baseline case, b) 12 MW balanced injected beam power, c) mixed neutral beam energies, four at 90 keV, four at 100 keV, and four at 110 keV, and d) 12 MW all co injected beams viewed from the +2.0 m sightline and 12 MW all counter injected beams viewed from the -2.0 m sightline. All other parameters are from the TFTR energetic ion mode baseline discharge.

Figure 17. Plan-view schematic of the TFTR showing the arrangement of the charge exchange analyzer arrays and the neutral beam injectors.

Figure 18. Measured deuterium spectra in the energy range of 50-200 keV during co-injection of deuterium neutral beams from 4.0-6.0 s into a deuterium plasma.

Figure 19. Deuterium charge exchange spectrum at t=5.5 s and the simultaneously measured neutron- and gamma-induced noise level. A linear least-squares fit to the data (open circles) in the energy range of E=124-187 keV yields T_{eff} =16.2 keV.

Figure 20. Comparison of the central ion temperature from charge exchange corrected for toroidal rotation effects (circles) with horizontal X-ray crystal Doppler broadening data (squares). The central rotation velocity in the case was 6.8×19^5 m/s. The upper dashed curve corresponds to the charge exchange data without correction for toroidal rotation. The lower curves show the total injected beam power, the line-integral electron density from the 1-mm interferometer, and the central electron temperature from the Michelson interferometer renormalized to the Thomson scattering measurement at t=5.5 s.

Figure 21. Comparison of the central ion temperature measured by charge exchange (solid circles) and X-ray crystal Doppler broadening (open circles) for a discharge with low toroidal rotation velocity ($|\vec{v}_\phi| \leq 1.5 \times 10^5$ m/s). The toroidal rotation correction to the charge exchange data is small ($\lesssim$7%) and has not been applied to the data as shown.

Figure 22. F(a,b) to be used in analysis of the effects of toroidal rotation on the high ion energy spectra obtained from TFTR discharges during unbalanced neutral beam injection. F is calculated for $6 < a < 11$ and for $6 < b < 20$.

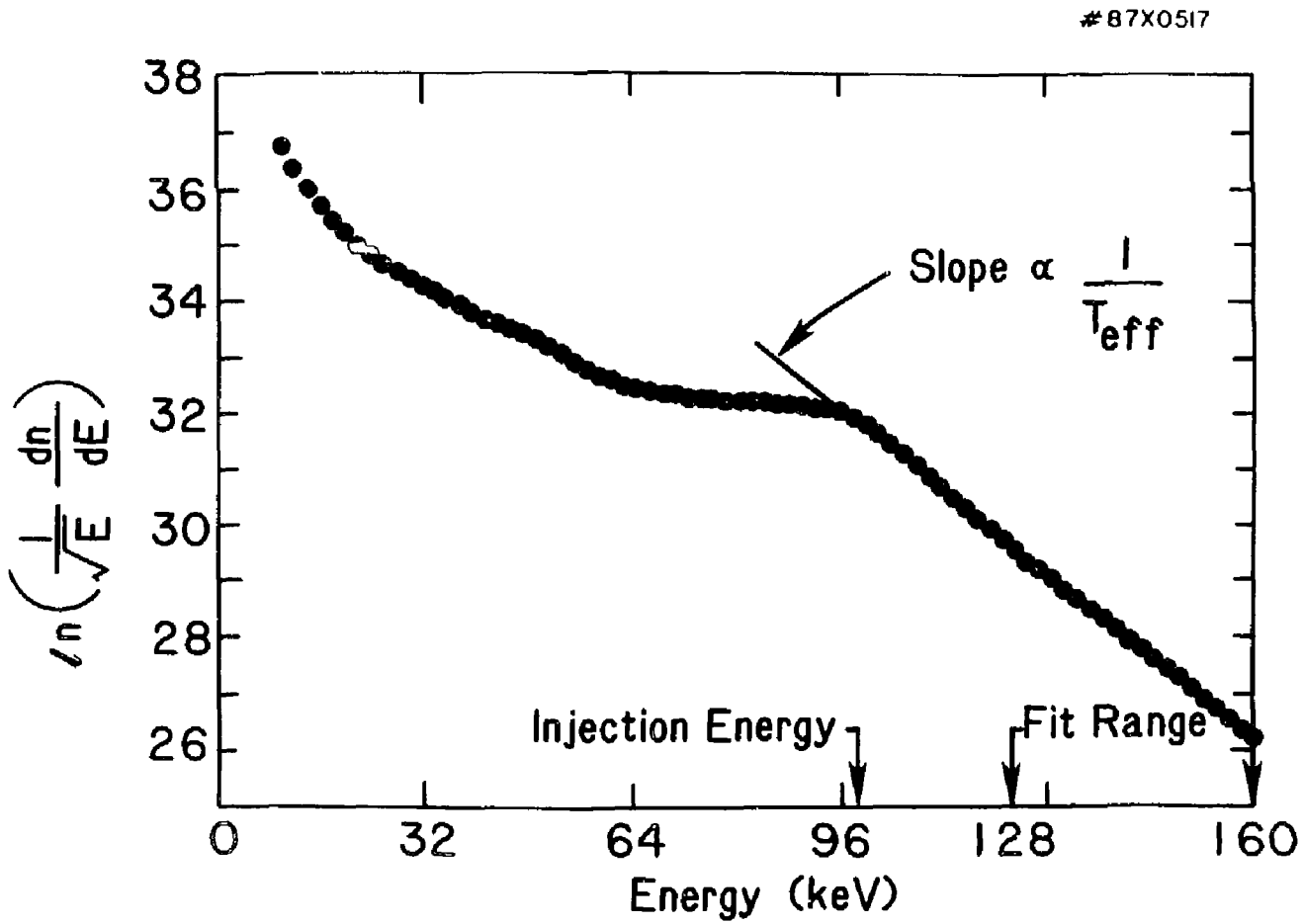
#87X0517
38
36
34
32
30
28
26
$\ln\left(\frac{1}{\sqrt{E}}\frac{dn}{dE}\right)$
Slope α $\frac{1}{T_{eff}}$
Injection Energy
Fit Range
0
32
64
96
128
160
Energy (keV)

Fig. 1

#87X0512

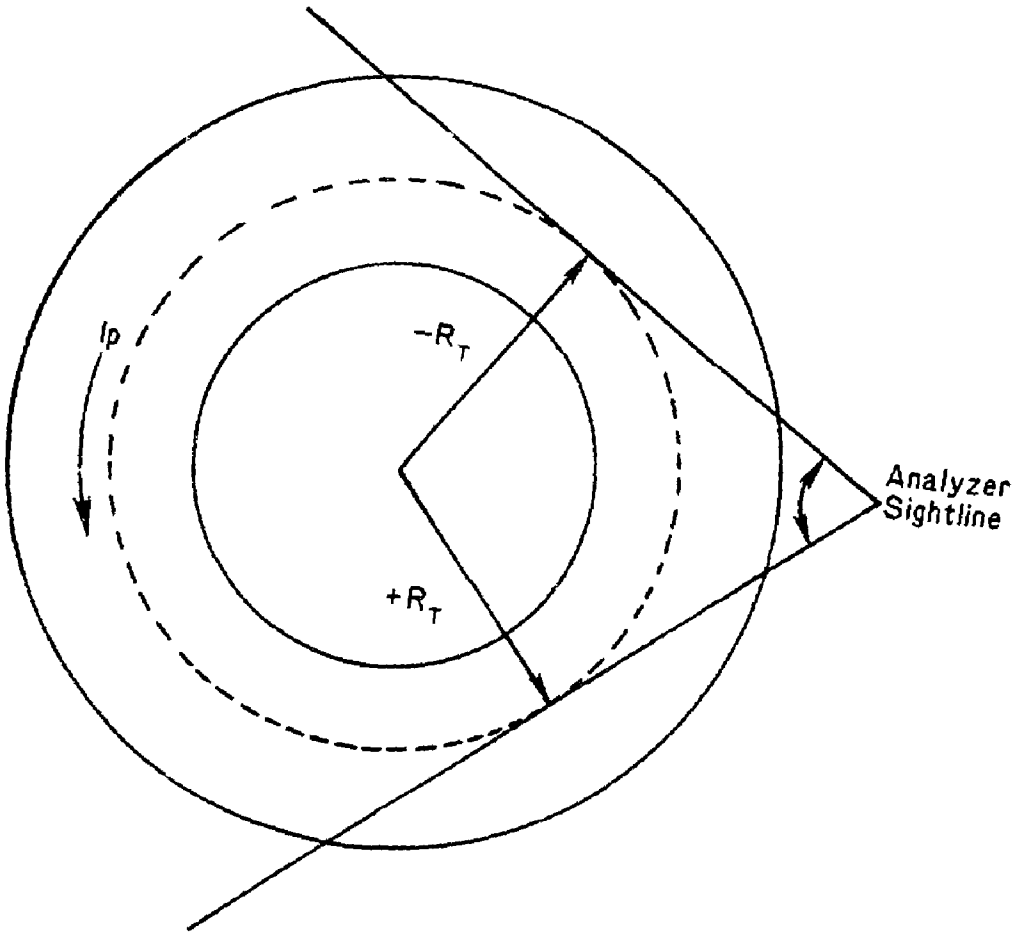

Fig. 2

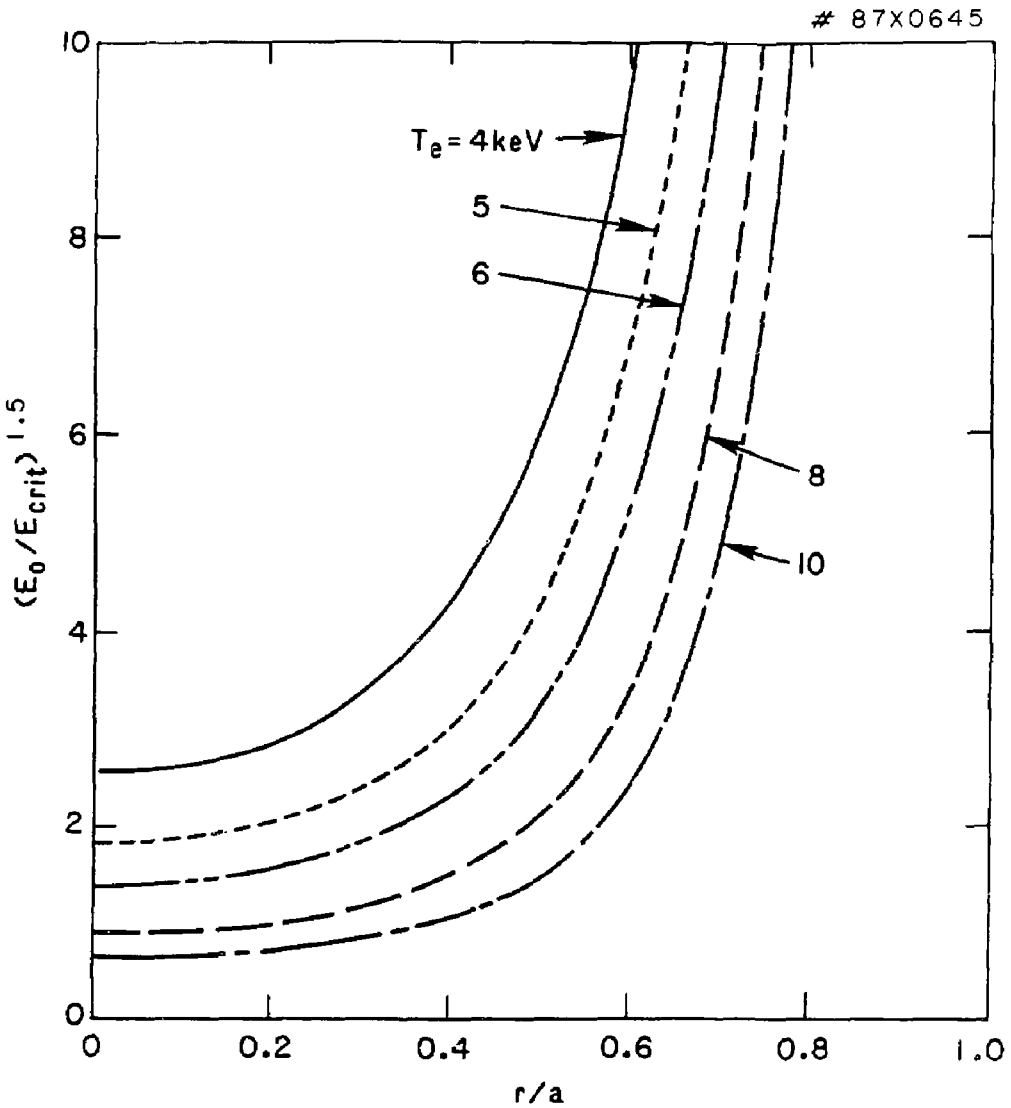

Fig. 3

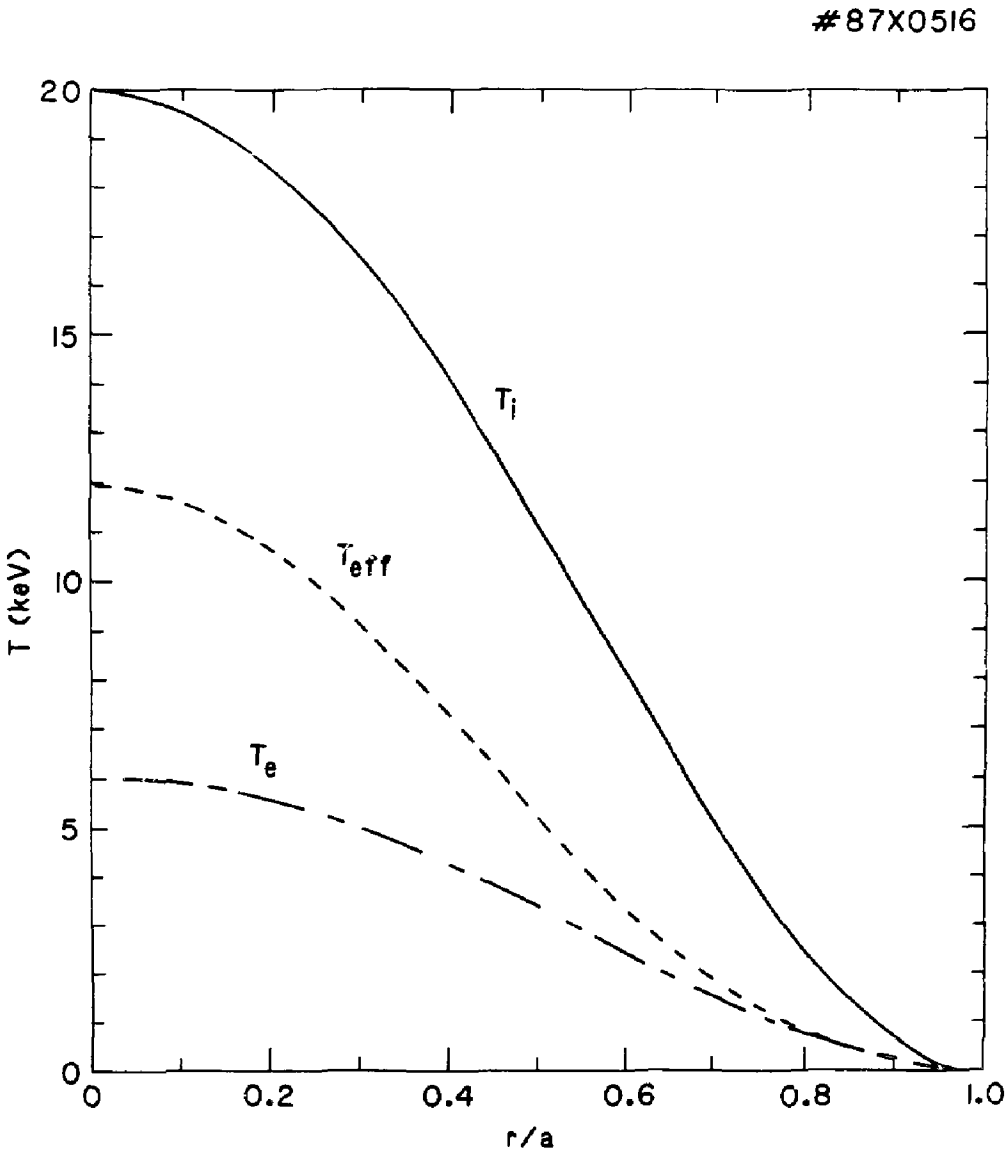

Fig. 4

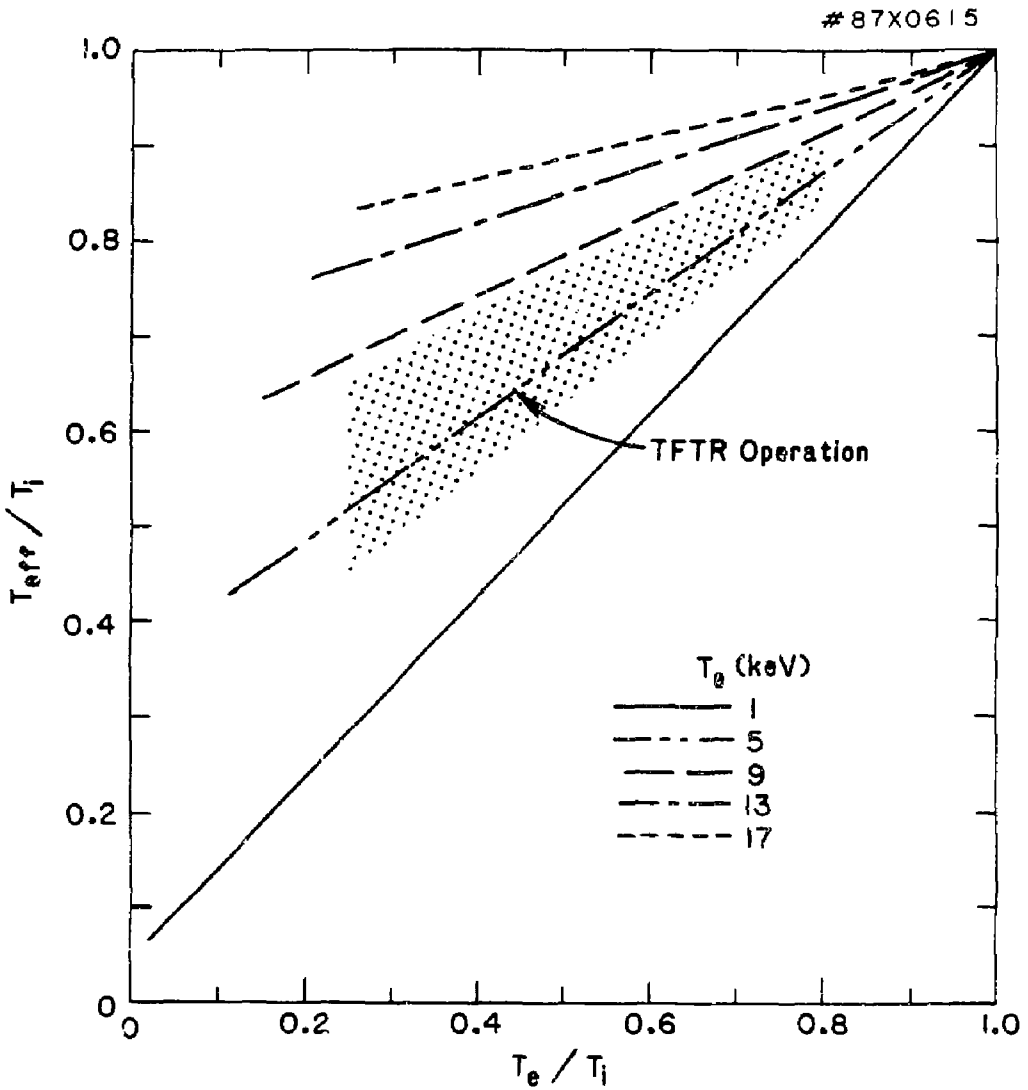
#87X0615
1.0
0.8
0.6
0.4
0.2
0
0
0.2
0.4
0.6
0.8
1.0
T_{eff} / T_i
T_e / T_i
TFTR Operation
T_e (keV)
1
5
9
13
17

Fig. 5

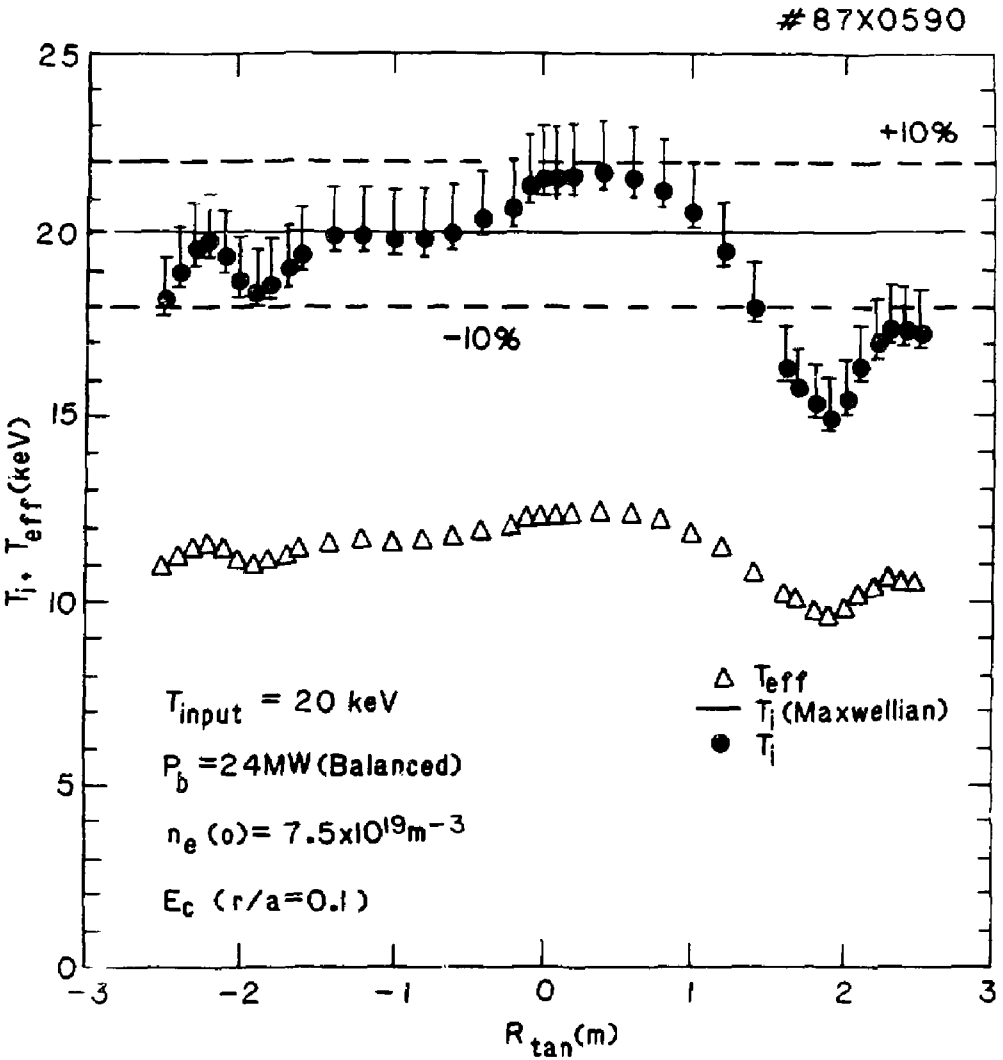
#87X0590
+10%
-10%
T_{input} = 20 keV
P_b =24MW(Balanced)
n_e (o)= 7.5x10^{19}m^{-3}
E_c (r/a=0.1)
T_{eff}
T_i (Maxwellian)
T_i
T_i, T_{eff}(keV)
R_{tan}(m)
25
20
15
10
5
0
-3
-2
-1
0
1
2
3

Fig. 6

#87X0514

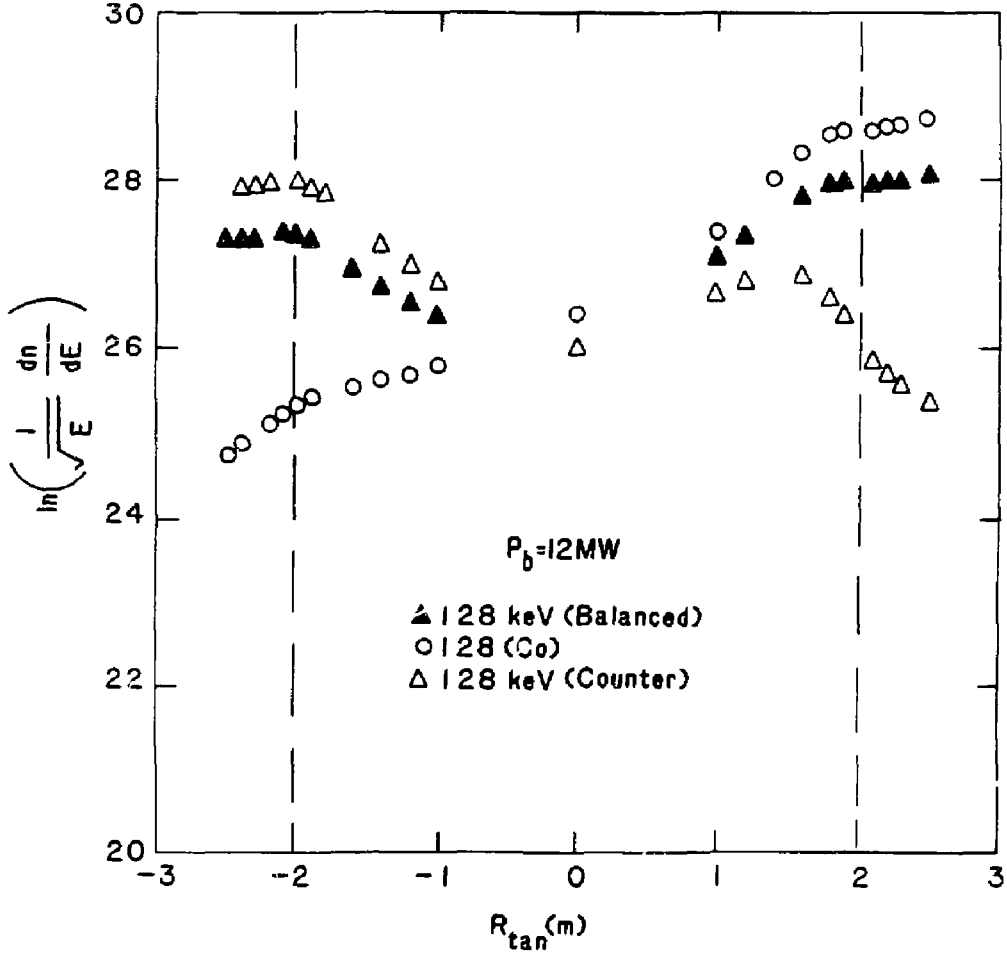

Fig. 7

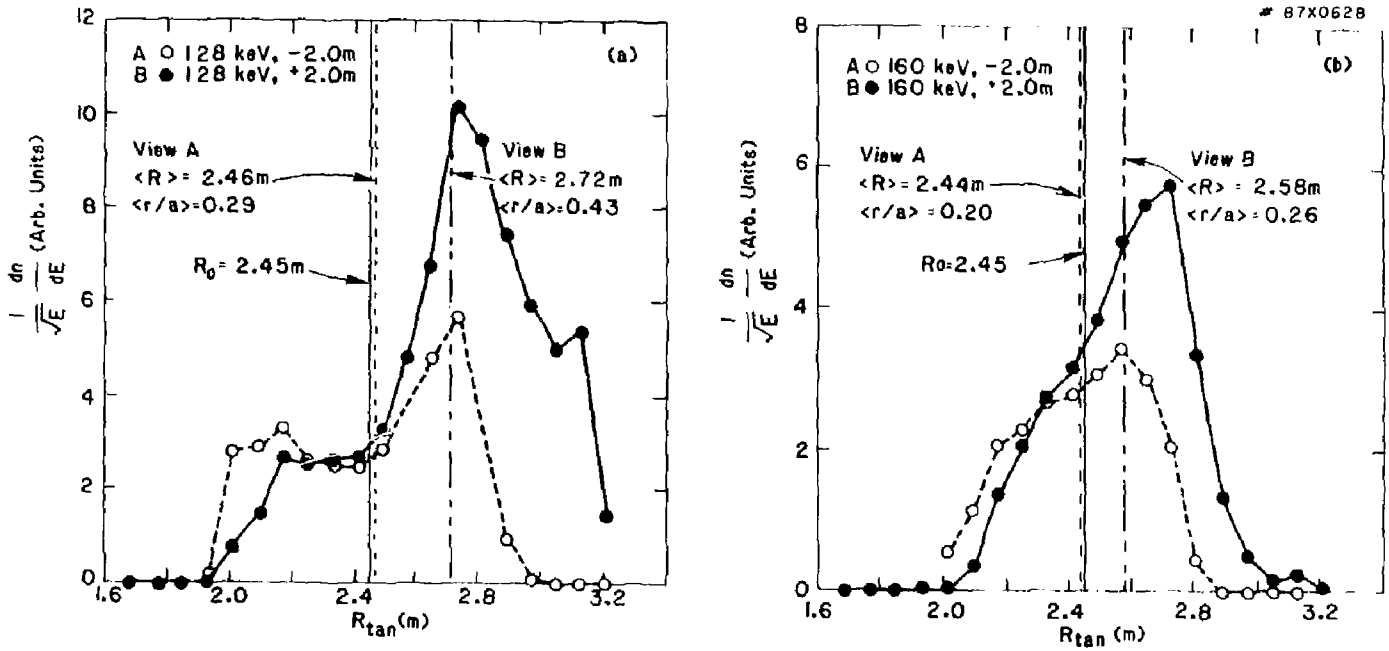
A ○ 128 keV, −2.0m
B ● 128 keV, +2.0m
(a)
View A
<R> = 2.46m
<r/a>=0.29
View B
<R>= 2.72m
<r/a>=0.43
R0 = 2.45m
1/√E dn/dE (Arb. Units)
Rtan(m)
# 87X0628
A ○ 160 keV, −2.0m
B ● 160 keV, +2.0m
(b)
View A
<R>= 2.44m
<r/a> = 0.20
View B
<R> = 2.58m
<r/a> = 0.26
Ro=2.45
1/√E dn/dE (Arb. Units)
Rtan (m)

Fig. 8

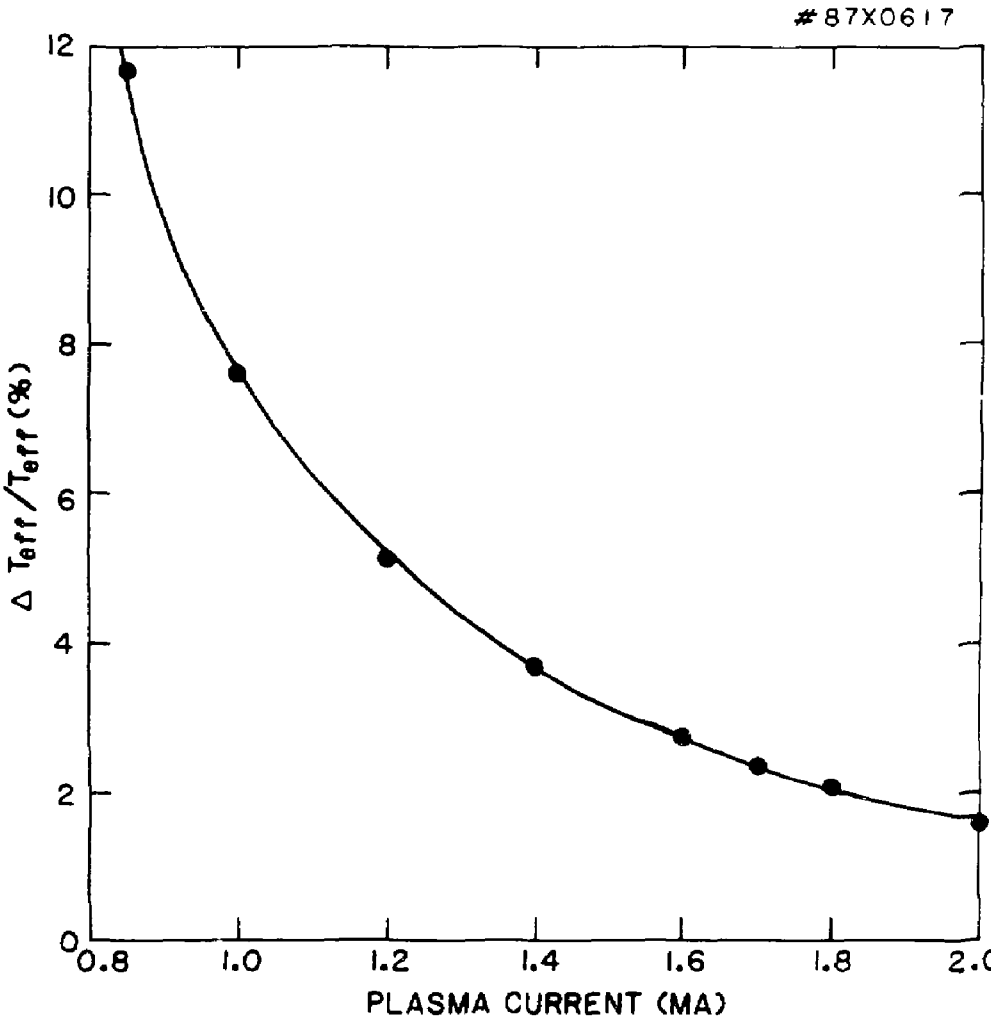
#87X0617
12
10
8
6
4
2
0
Δ Teff/Teff (%)
0.8
1.0
1.2
1.4
1.6
1.8
2.0
PLASMA CURRENT (MA)

Fig. 9

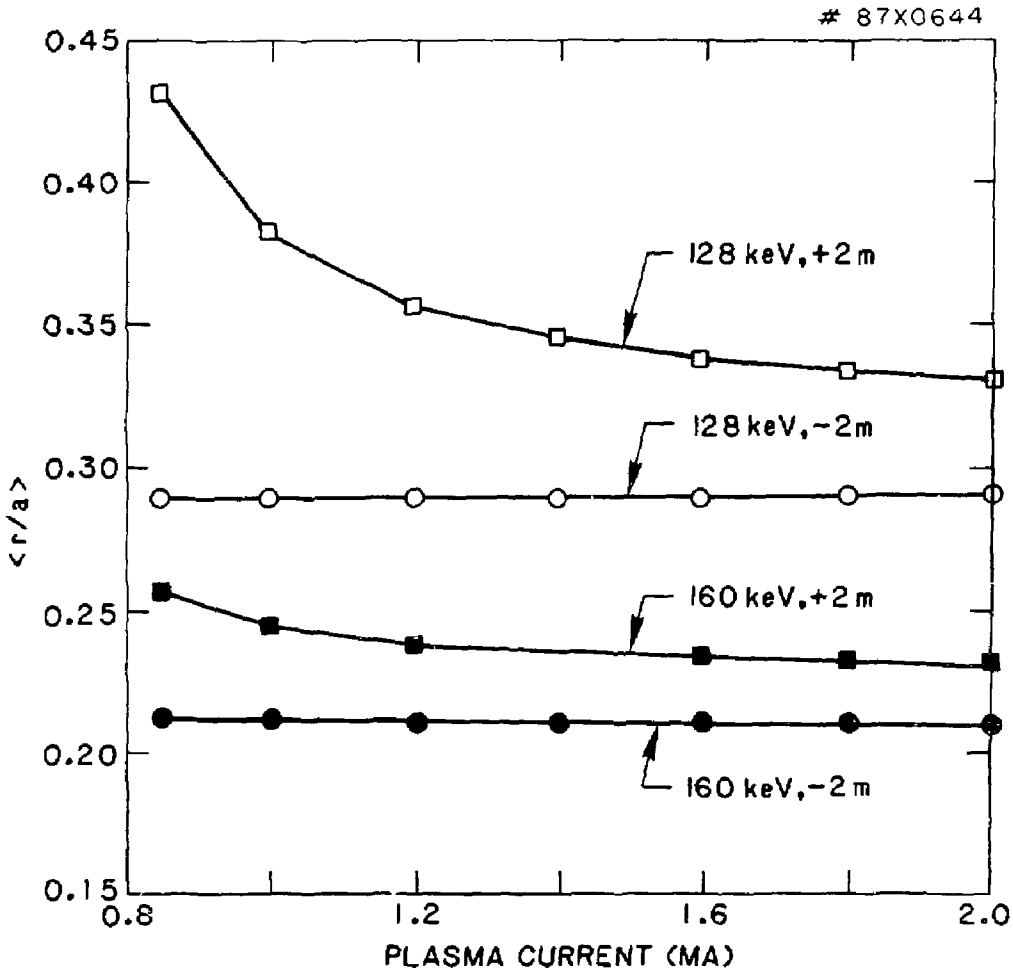
87X0644
0.45
0.40
0.35
0.30
0.25
0.20
0.15
<r/a>
128 keV, +2 m
128 keV, -2 m
160 keV, +2 m
160 keV, -2 m
0.8
1.2
1.6
2.0
PLASMA CURRENT (MA)

Fig. 10

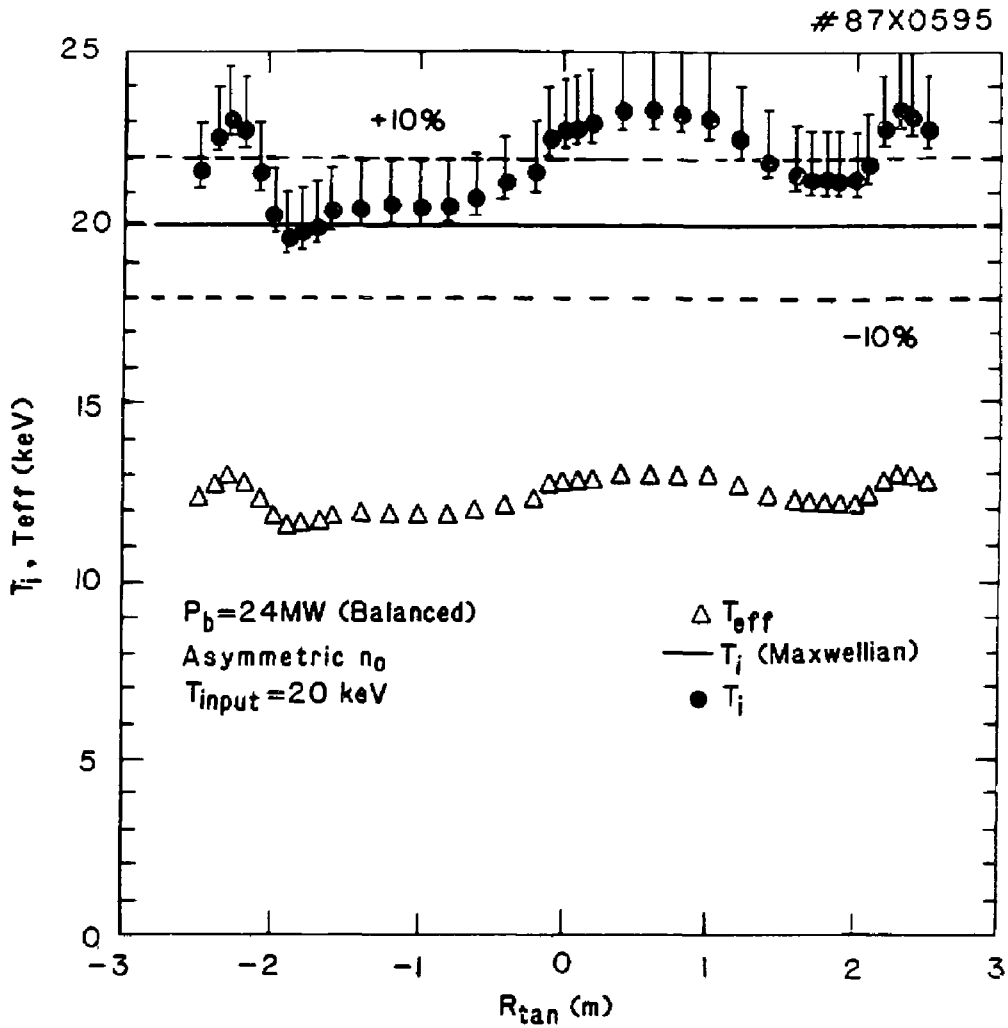
#87X0595
25
20
15
10
5
0
+10%
-10%
T_i, Teff (keV)
P_b=24MW (Balanced)
Asymmetric n_0
T_{input}=20 keV
Δ T_{eff}
T_i (Maxwellian)
T_i
-3
-2
-1
0
1
2
3
R_{tan} (m)

Fig. 11

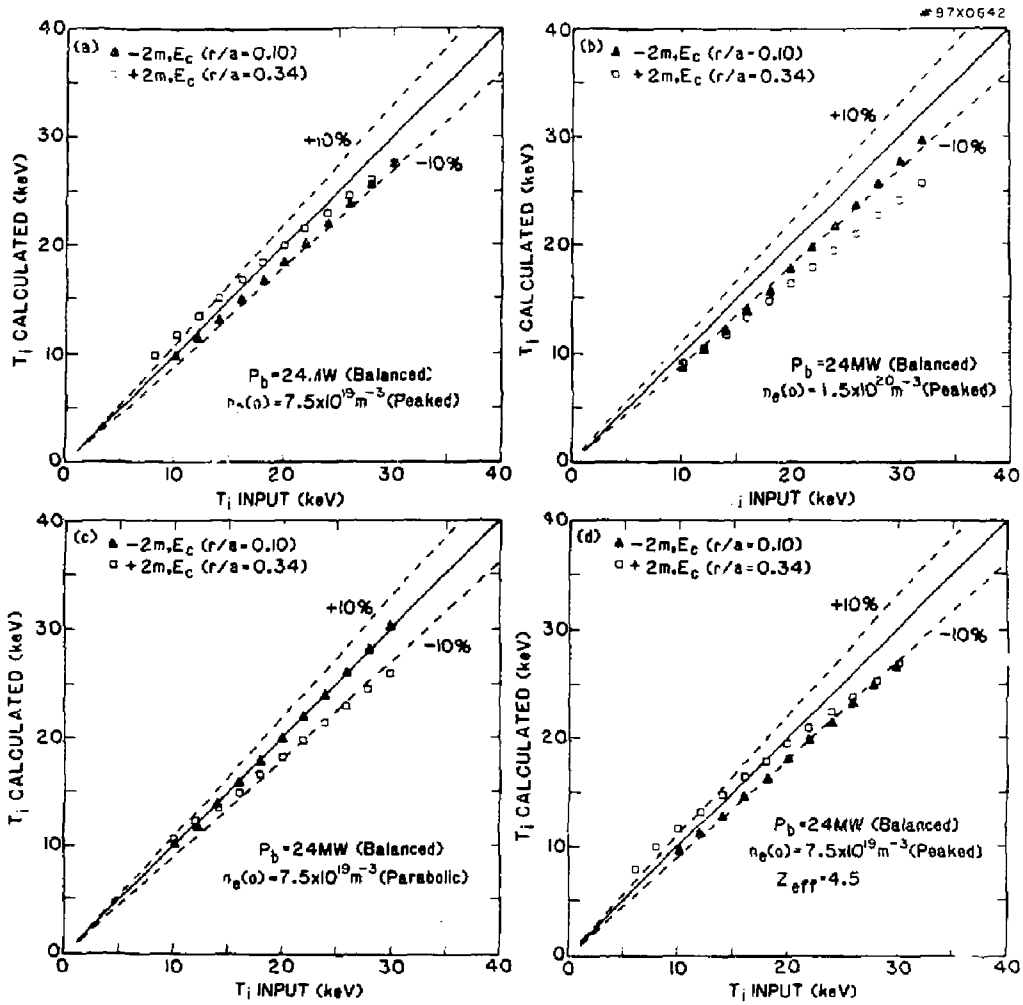
#97X0642
(a) ▲ −2m,Ec (r/a=0.10)
□ +2m,Ec (r/a=0.34)
+10%
−10%
Pb=24.4W (Balanced)
ne(o)=7.5x10^19m^-3(Peaked)
Ti CALCULATED (keV)
Ti INPUT (keV)
(b) ▲ −2m,Ec (r/a=0.10)
□ +2m,Ec (r/a=0.34)
+10%
−10%
Pb=24MW (Balanced)
ne(o)=1.5x10^20m^-3(Peaked)
Ti CALCULATED (keV)
Ti INPUT (keV)
(c) ▲ −2m,Ec (r/a=0.10)
□ +2m,Ec (r/a=0.34)
+10%
−10%
Pb=24MW (Balanced)
ne(o)=7.5x10^19m^-3(Parabolic)
Ti CALCULATED (keV)
Ti INPUT (keV)
(d) ▲ −2m,Ec (r/a=0.10)
□ +2m,Ec (r/a=0.34)
+10%
−10%
Pb=24MW (Balanced)
ne(o)=7.5x10^19m^-3(Peaked)
Zeff=4.5
Ti CALCULATED (keV)
Ti INPUT (keV)

Fig. 12

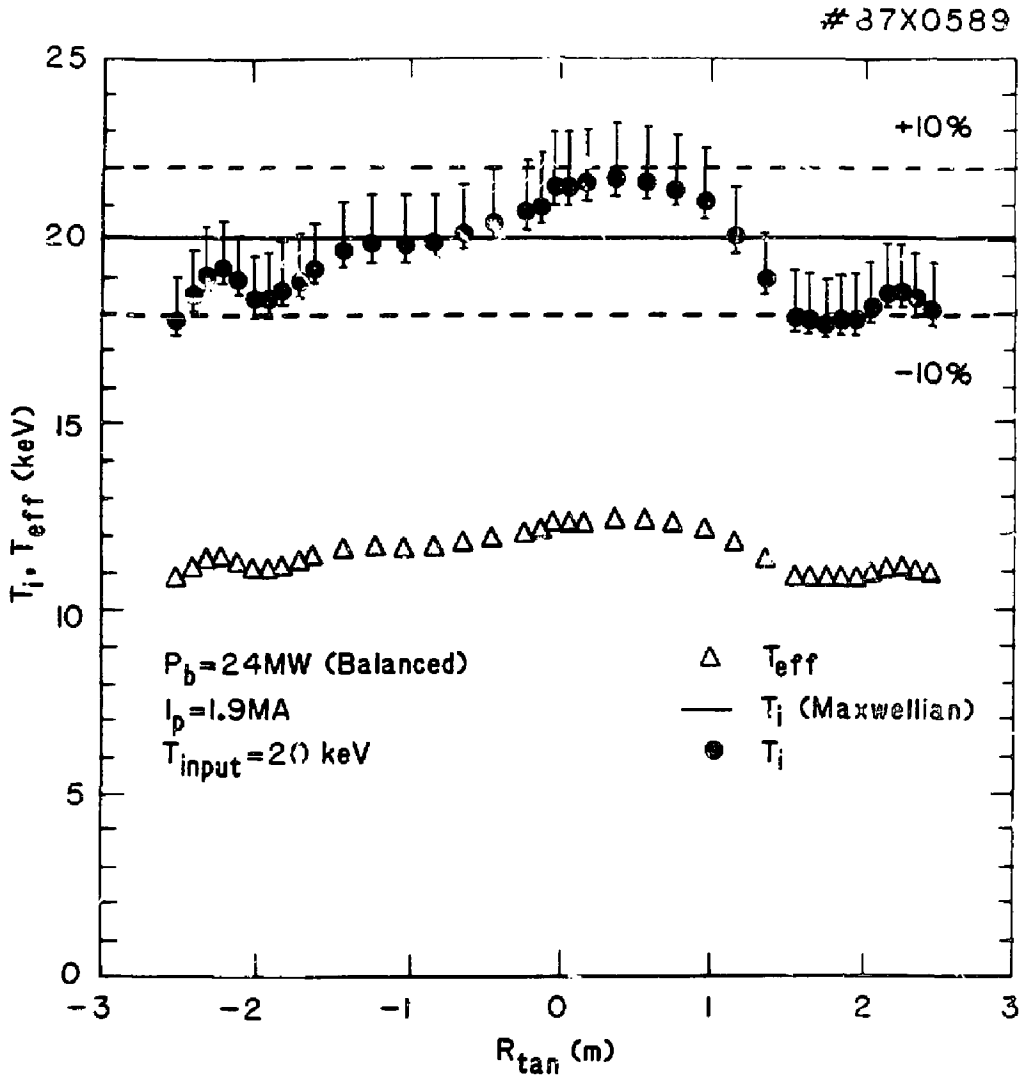
#87X0589
+10%
-10%
T_i, T_{eff} (keV)
P_b=24MW (Balanced)
I_p=1.9MA
T_{input}=20 keV
T_{eff}
T_i (Maxwellian)
T_i
R_{tan} (m)

Fig. 13

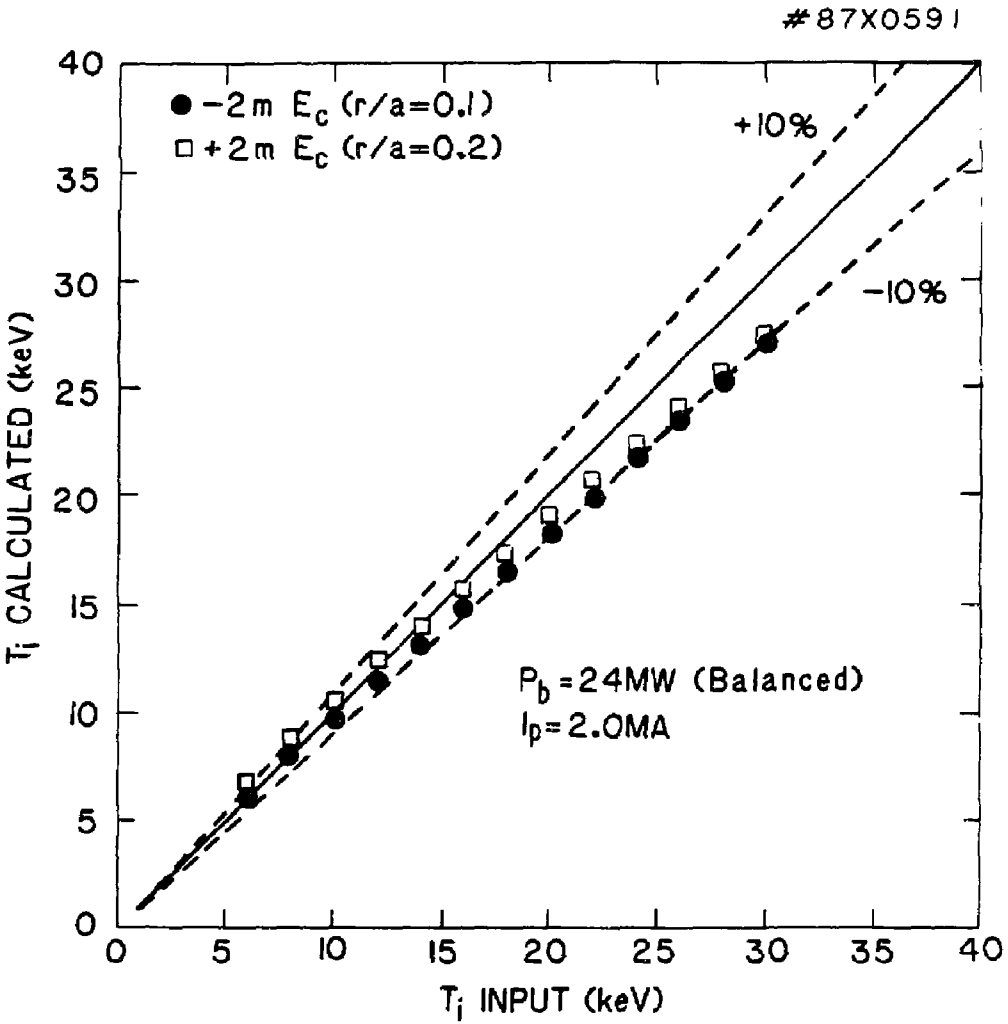
#87X0591
● −2m E_c (r/a=0.1)
□ +2m E_c (r/a=0.2)
+10%
−10%
P_b = 24MW (Balanced)
I_p = 2.0MA
T_i CALCULATED (keV)
T_i INPUT (keV)
0
5
10
15
20
25
30
35
40

Fig. 14

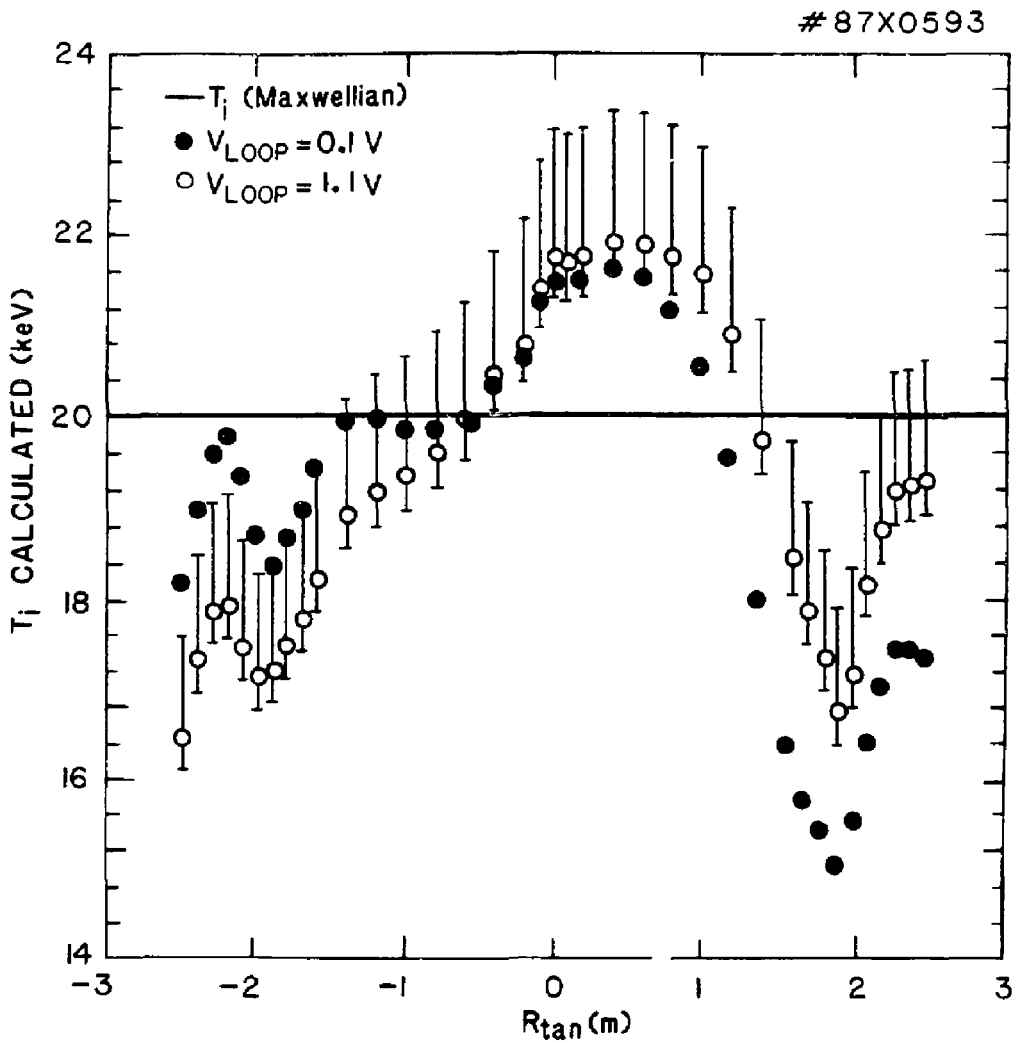
#87X0593
T_i (Maxwellian)
V_{LOOP} = 0.1 V
V_{LOOP} = 1.1 V
T_i CALCULATED (keV)
24
22
20
18
16
14
-3
-2
-1
0
1
2
3
R_{tan} (m)

Fig. 15

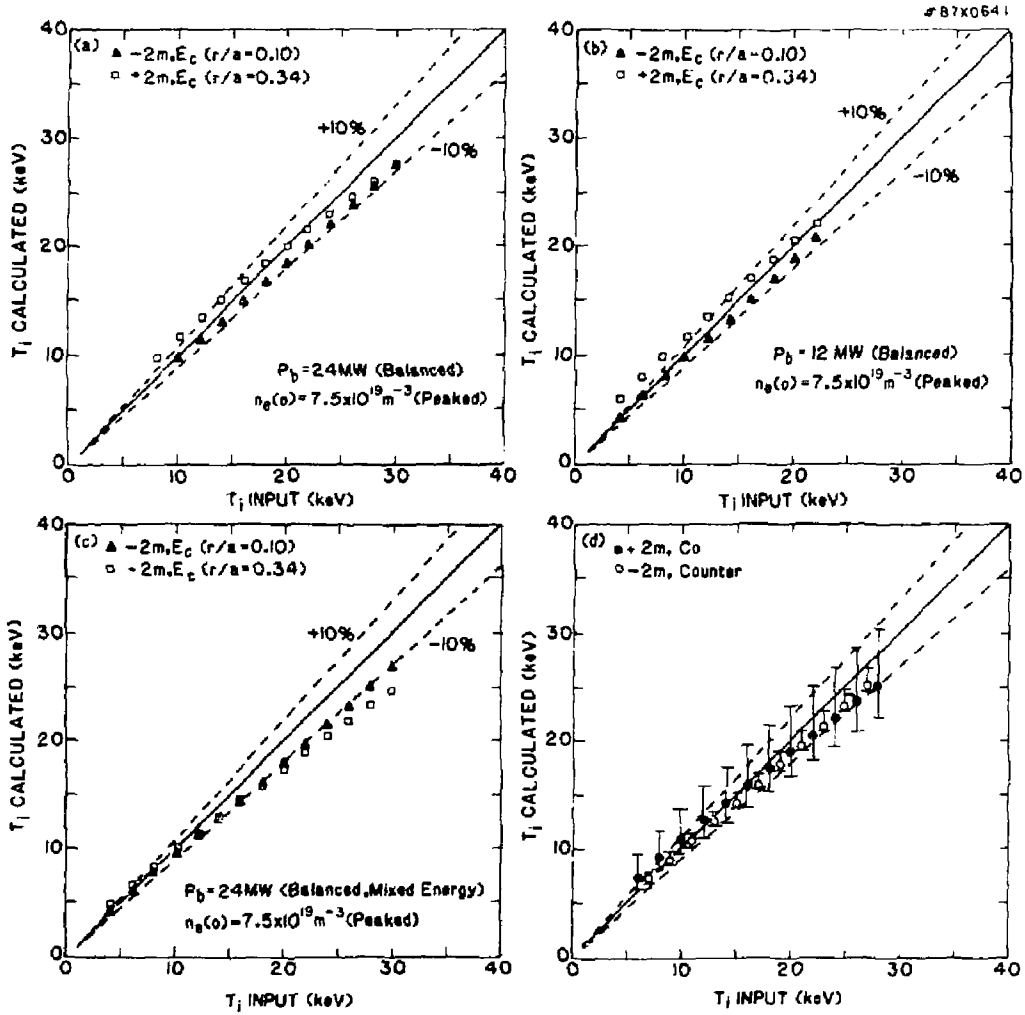
#87X0641
(a) ▲ −2m, E_c (r/a=0.10)
□ +2m, E_c (r/a=0.34)
+10%
−10%
P_b=24MW (Balanced)
$n_e(o)$=7.5x10^{19}m^{-3}(Peaked)
T_i CALCULATED (keV)
T_i INPUT (keV)
(b) ▲ −2m, E_c (r/a=0.10)
□ +2m, E_c (r/a=0.34)
+10%
−10%
P_b = 12 MW (Balanced)
$n_e(o)$=7.5x10^{19}m^{-3}(Peaked)
T_i CALCULATED (keV)
T_i INPUT (keV)
(c) ▲ −2m, E_c (r/a=0.10)
□ +2m, E_c (r/a=0.34)
+10%
−10%
P_b=24MW (Balanced, Mixed Energy)
$n_e(o)$=7.5x10^{19}m^{-3}(Peaked)
T_i CALCULATED (keV)
T_i INPUT (keV)
(d) ● +2m, Co
○ −2m, Counter
T_i CALCULATED (keV)
T_i INPUT (keV)

Fig. 16

BEAM	R_{tan}(m)
2A	−1.73
2B	−1.99
2C	−2.23
3A	2.53
3B	2.31
3C	2.07
4A	2.84
4B	2.63
4C	2.41
5A	2.23
5B	1.99
5C	1.75

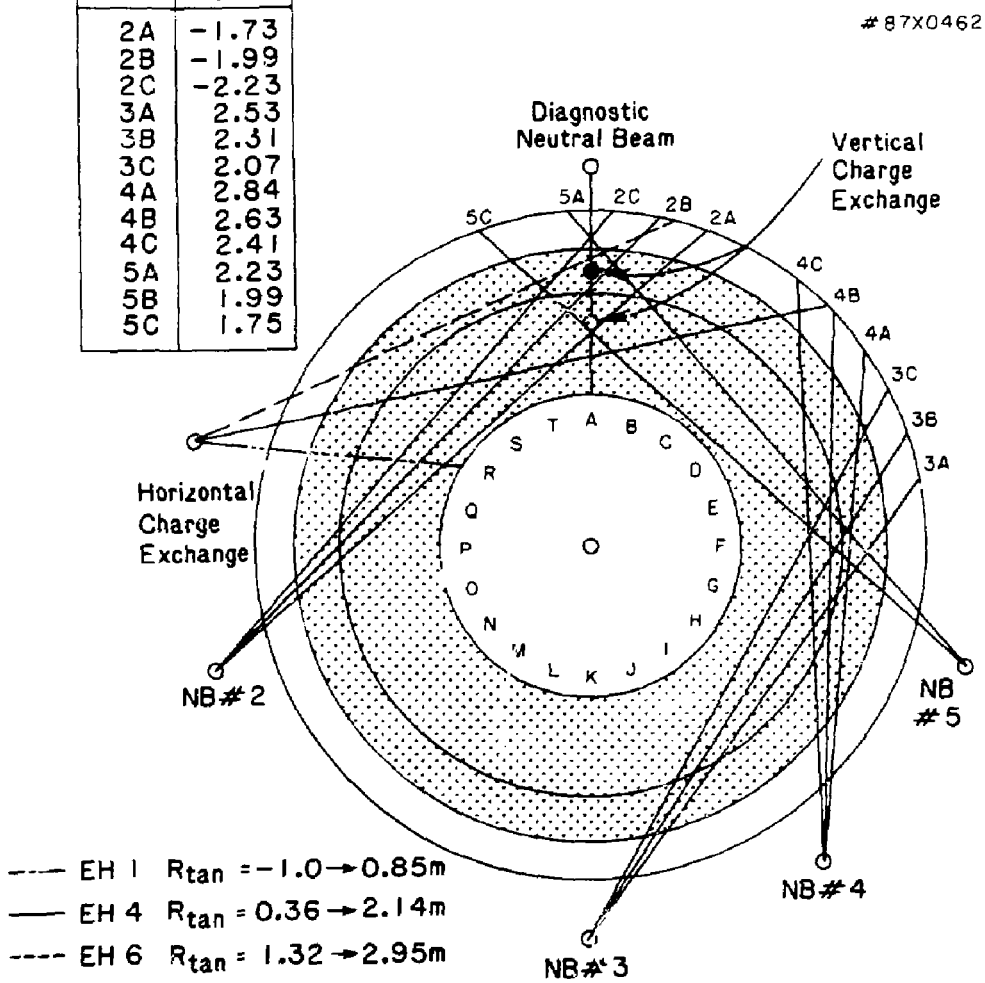

Fig. 17

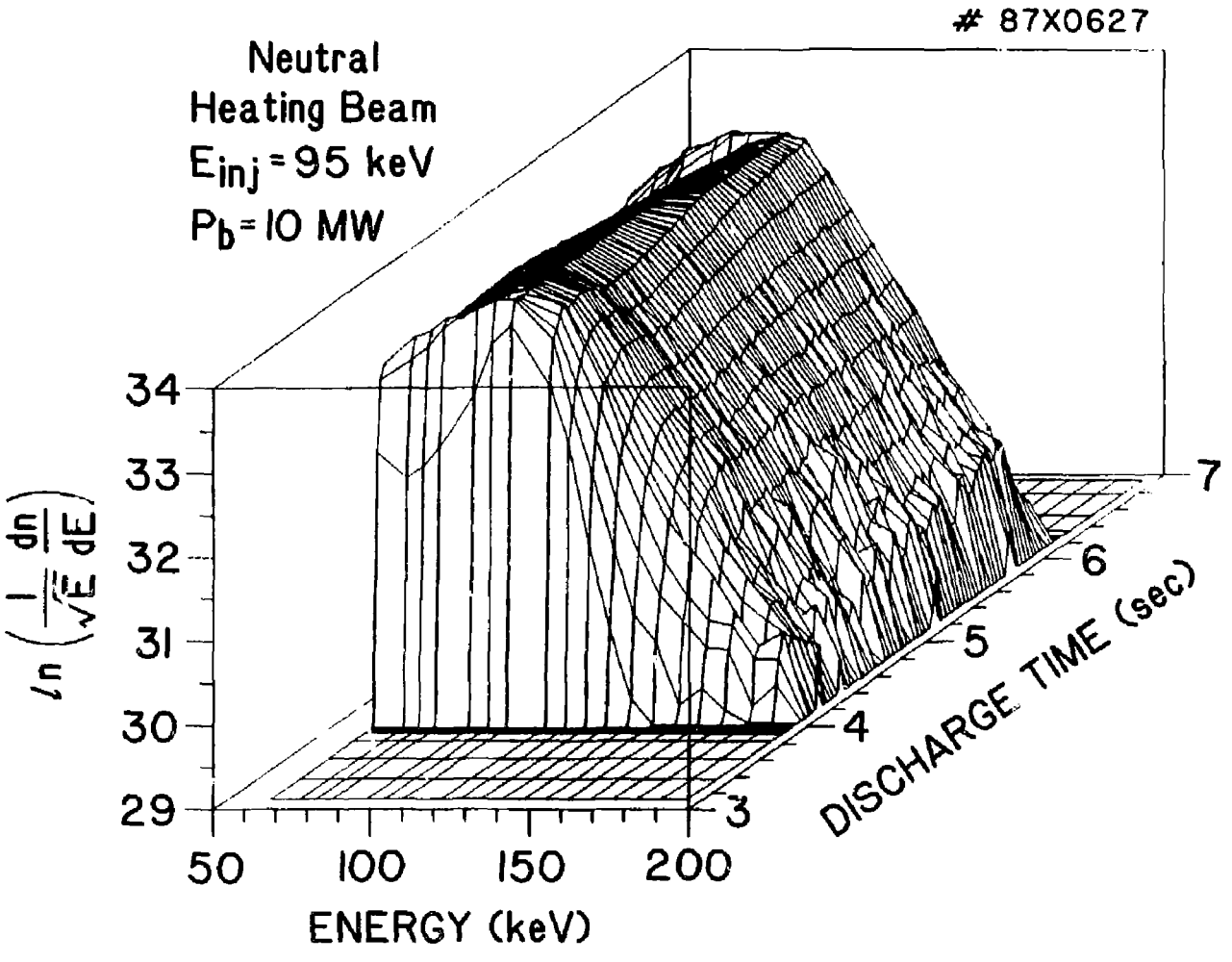
87X0627
Neutral
Heating Beam
E_{inj} = 95 keV
P_b = 10 MW
34
33
32
31
30
29
$\ln\left(\frac{1}{\sqrt{E}}\frac{dn}{dE}\right)$
50
100
150
200
ENERGY (keV)
3
4
5
6
7
DISCHARGE TIME (sec)

Fig. 18

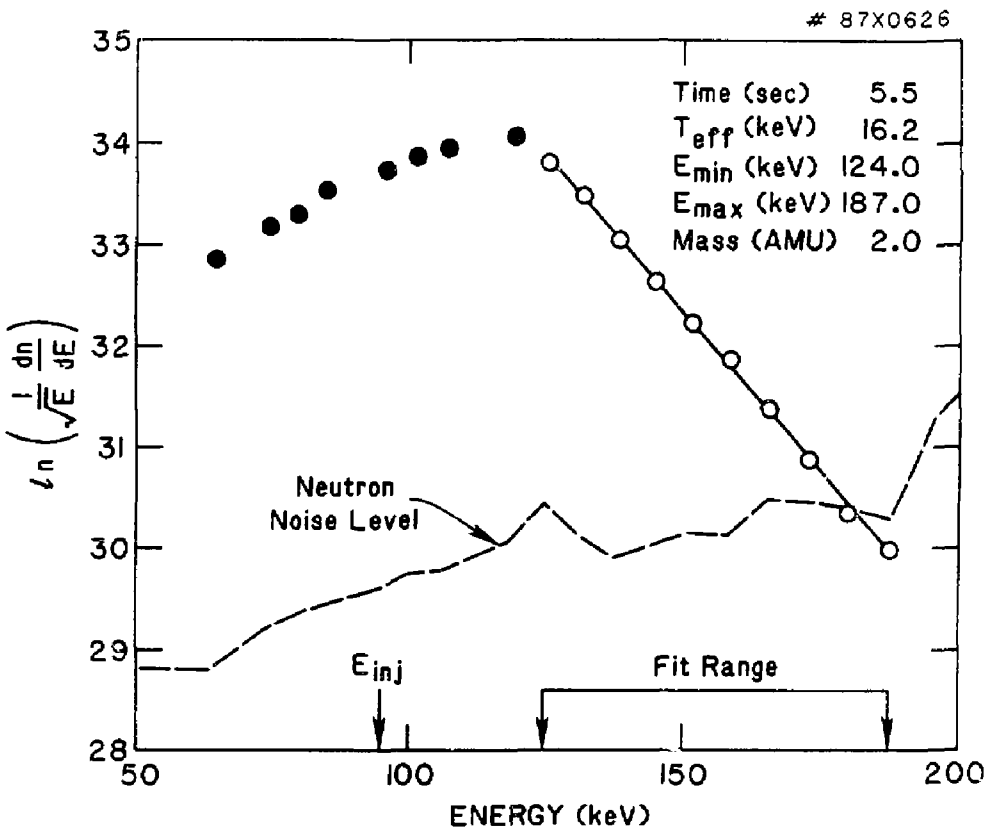
87X0626
Time (sec) 5.5
T_{eff} (keV) 16.2
E_{min} (keV) 124.0
E_{max} (keV) 187.0
Mass (AMU) 2.0
Neutron Noise Level
E_{inj}
Fit Range
$\ln\left(\frac{1}{\sqrt{E}}\frac{dn}{dE}\right)$
ENERGY (keV)
35
34
33
32
31
30
29
28
50
100
150
200

Fig. 19

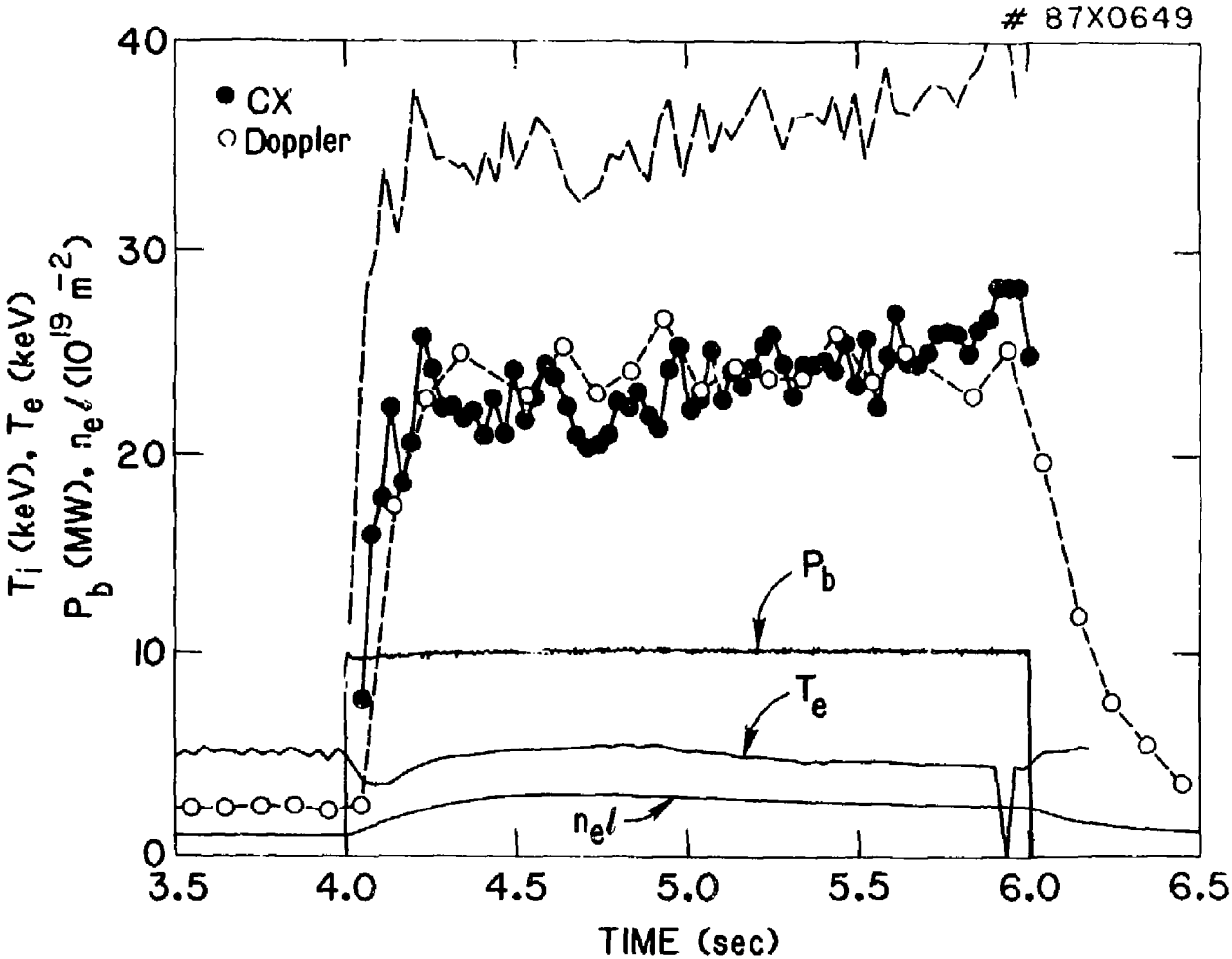
87X0649
CX
Doppler
T_i (keV), T_e (keV)
P_b (MW), $n_e l$ (10^{19} m^{-2})
40
30
20
10
0
P_b
T_e
$n_e l$
3.5
4.0
4.5
5.0
5.5
6.0
6.5
TIME (sec)

Fig. 20

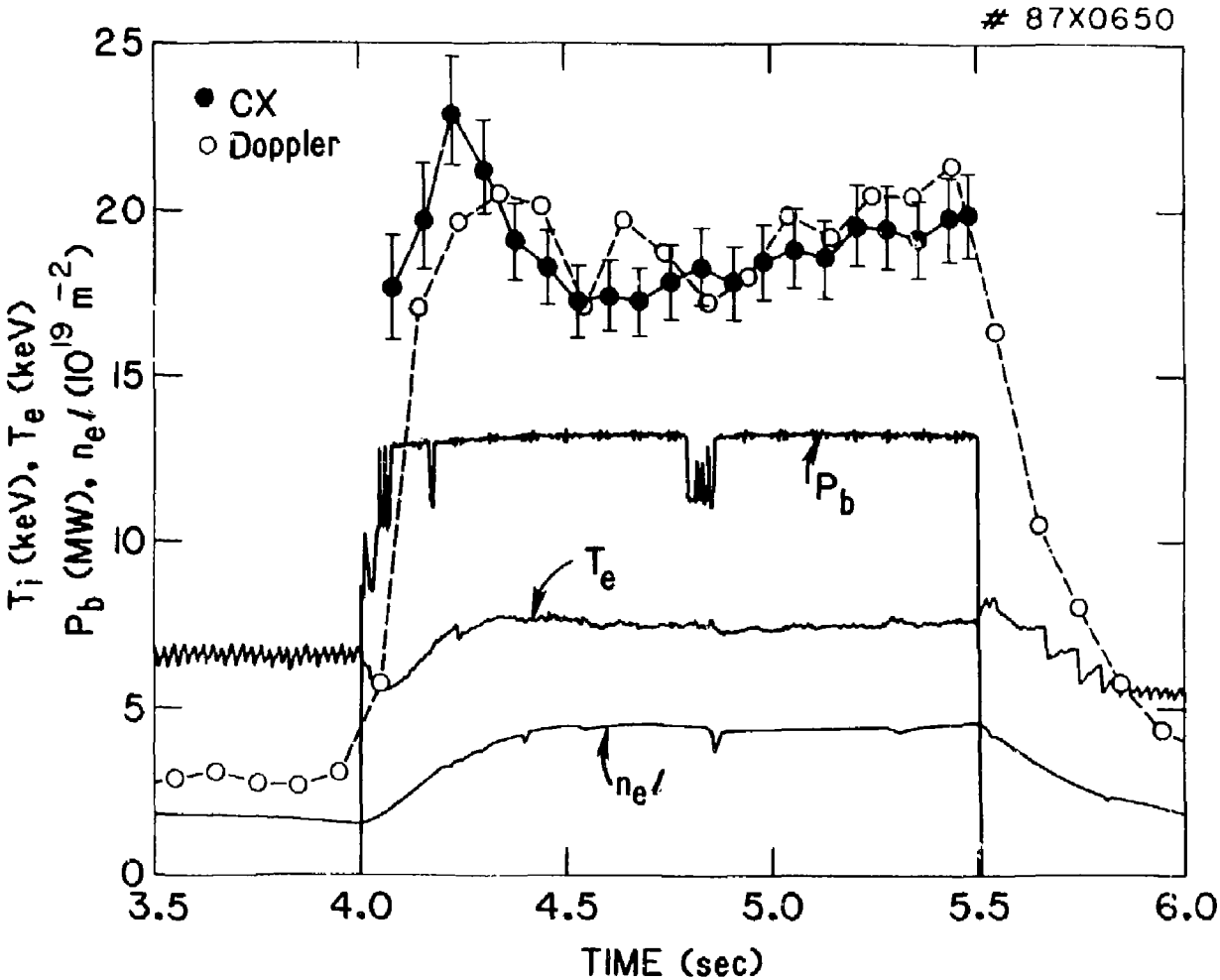
87X0650
CX
Doppler
T_i (keV), T_e (keV)
P_b (MW), n_e / (10^{19} m^{-2})
P_b
T_e
n_e/
TIME (sec)
0
5
10
15
20
25
3.5
4.0
4.5
5.0
5.5
6.0

Fig. 21

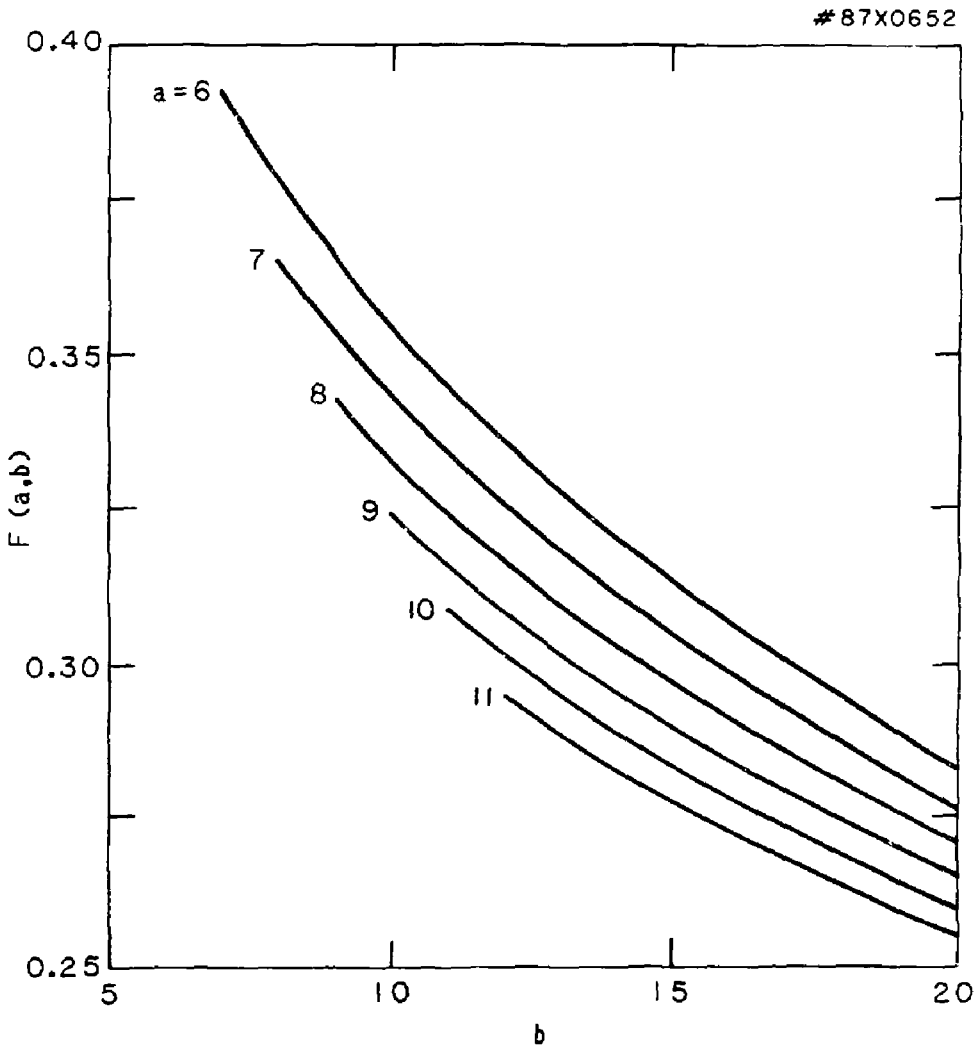

Fig. 22

EXTERNAL DISTRIBUTION IN ADDITION TO UC-20

Dr. Frank J. Paoloni, Univ of Wollongong, AUSTRALIA
Prof. M.H. Brennan, Univ Sydney, AUSTRALIA
Plasma Research Lab., Australian Nat. Univ., AUSTRALIA
Prof. I.R. Jones, Flinders Univ., AUSTRALIA
Prof. F. Cap, Inst Theo Phys, AUSTRIA
Prof. M. Heindler, Institut fur Theoretische Physik, AUSTRIA
M. Goossens, Astronomisch Instituut, BELGIUM
Ecole Royale Militaire, Lab de Phys Plasmas, BELGIUM
Com. of European, Dg XII Fusion Prog, BELGIUM
Prof. R. Boucique, Laboratorium voor Natuurkunde, BELGIUM
Dr. P.H. Sakanaka, Univ Estadual, BRAZIL
Instituto De Pesquisas Espaciasi-INPE, BRAZIL
Library, Atomic Energy of Canada Limited, CANADA
Dr. M.P. Bachynski, MPB Technologies, Inc., CANADA
Dr. H.M. Skarsgard, Univ of Saskatchewan, CANADA
Dr. H. Barnard, University of British Columbia, CANADA
Prof. J. Teichmann, Univ. of Montreal, CANADA
Prof. S.R. Sreenivasan, University of Calgary, CANADA
Prof. Tudor W. Johnston, INRS-Energie, CANADA
Dr. C.R. James, Univ. of Alberta, CANADA
Dr. Peter Lukac, Komenskeho Univ, CZECHOSLOVAKIA
The Librarian, Culham Laboratory, ENGLAND
Mrs. S.A. Hutchinson, JET Library, ENGLAND
C. Mouttet, Lab. de Physique des Milieux Ionises, FRANCE
J. Radet, CEN/CADARACHE - Bat 506, FRANCE
Dr. Tom Mual, Academy Bibliographic, HONG KONG
Preprint Library, Cent Res Inst Phys, HUNGARY
Dr. B. Dasgupta, Saha Inst, INDIA
Dr. R.K. Chhajlani, Vikram Univ. INDIA
Dr. P. Kaw, Institute for Plasma Research, INDIA
Dr. Phillip Rosenau, Israel Inst Tech, ISRAEL
Prof. S. Cuperman, Tel Aviv University, ISRAEL
Librarian, Int'l Ctr Theo Phys, ITALY
Prof. G. Rostagni, Univ Di Padova, ITALY
Miss Clelia De Palo, Assoc EURATOM-ENEA, ITALY
Biblioteca, del CNR EURATOM, ITALY
Dr. M. Yamato, Toshiba Res & Dev, JAPAN
Prof. I. Kawakami, Atomic Energy Res. Institute, JAPAN
Prof. Kyoji Nishikawa, Univ of Hiroshima, JAPAN
Direc. Dept. Lg. Tokamak Res. JAERI, JAPAN
Prof. Satoshi Itoh, Kyushu University, JAPAN
Research Info Center, Nagoya University, JAPAN
Prof. S. Tanaka, Kyoto University, JAPAN
Library, Kyoto University, JAPAN
Prof. Nobuyuki Inoue, University of Tokyo, JAPAN
S. Mori, JAERI, JAPAN
M.H. Kim, Korea Advanced Energy Research Institute, KOREA
Prof. D.I. Choi, Adv. Inst Sci & Tech, KOREA
Prof. B.S. Liley, University of Waikato, NEW ZEALAND
Institute of Plasma Physics, PEOPLE'S REPUBLIC OF CHINA
Librarian, Institute of Phys., PEOPLE'S REPUBLIC OF CHINA
Library, Tsing Hua University, PEOPLE'S REPUBLIC OF CHINA
Z. Li, Southwest Inst. Physics, PEOPLE'S REPUBLIC OF CHINA
Prof. J.A.C. Cabral, Inst Superior Tecn, PORTUGAL
Dr. Octavian Petrus, AL I CUZA University, ROMANIA
Dr. Johan de Villiers, Plasma Physics, AEC, SO AFRICA
Prof. M.A. Hellberg, University of Natal, SO AFRICA
Fusion Div. Library, JEN, SPAIN
Dr. Lennart Stenflo, University of UMEA, SWEDEN
Library, Royal Inst Tech, SWEDEN
Prof. Hans Wilhelmson, Chalmers Univ Tech, SWEDEN
Centre Phys des Plasmas, Ecole Polytech Fed, SWITZERLAND
Bibliotheek, Fom-Inst Voor Plasma-Fysica, THE NETHERLANDS
Dr. O.D. Ryutov, Siberian Acad Sci, USSR
Dr. G.A. Eliseev, Kurchatov Institute, USSR
Dr. V.A. Glukhikh, Inst Electro-Physical, USSR
Dr. V.T. Tolok, Inst. Phys. Tech. USSR
Dr. L.M. Kovrizhnykh, Institute Gen. Physics, USSR
Prof. T.J.M. Boyd, Univ College N Wales, WALES
Nuclear Res. Establishment, Julich Ltd., W. GERMANY
Bibliothek, Inst. Fur Plasmaforschung, W. GERMANY
Dr. K. Schindler, Ruhr Universitat, W. GERMANY
ASDEX Reading Rm, IPP/Max-Planck-Institut fur Plasmaphysik, W. GERMANY
Librarian, Max-Planck Institut, W. GERMANY
Prof. R.K. Janev, Inst Phys, YUGOSLAVIA